

Discovery of 3,3'-(2,4-Diaminopteridine-6,7-diyl)diphenol as an Isozyme-Selective Inhibitor of PI3K for the Treatment of Ischemia Reperfusion Injury Associated with Myocardial Infarction

Moorthy S. S. Palanki,*[†] Elena Dneprovskaja,[†] John Doukas,[†] Richard M. Fine,[‡] John Hood,[†] Xinshan Kang,[‡] Dan Lohse,[†] Michael Martin,[†] Glenn Noronha,[†] Richard M. Soll,[†] Wolfgang Wrasidlo,[†] Shiyin Yee,[†] and Hong Zhu[†]

TargeGen Inc., 9380 Judicial Drive, San Diego California 92121, and BioPredict, Inc., Suite 201, 660 Kinderkamack Road, Oradell, New Jersey 07649

Received October 19, 2005

In studies aimed toward identifying effective and safe inhibitors of kinase signaling cascades that underlie ischemia/reperfusion (I/R) injury, we synthesized a series of pteridines and pyridopyrazines. The design strategy was inspired by the examination of naturally occurring PI3K inhibitors such as wortmannin and quercetin, and building a pharmacophore-based model used for optimization. Structural modifications led to hybrid molecules which incorporated aminopyrimidine and aminopyridine moieties with ATP mimetic characteristics into the pharmacophore motifs to modulate kinase affinity and selectivity. Elaborations involving substitutions of the 2 and 4 positions of the pyrimidine or pyridine ring and the 6 and 7 positions of the central pyrazine ring resulted in *in vivo* activity profiles which identified potent inhibitors of vascular endothelial growth factor (VEGF) induced vascular leakage. Pathway analysis identified a diaminopteridine-diphenol as a potent and selective phosphatidylinositol-3-kinase (PI3K) inhibitor. The structure–activity relationship studies of various analogues of diaminopteridine-diphenol-based on biochemical assays resulted in potent inhibitors of PI3K.

Introduction

The vascular endothelium plays a key role in physiological homeostasis by regulating functions such as blood plasma–interstitial fluid balance via vascular permeability control. Ischemic tissue damage results in part from the disruption of this homeostatic balance. As first shown by Dvorak et al.,¹ an ischemic environment triggers upregulation of vascular endothelial growth factor (VEGF) expression, followed by VEGF-mediated vascular leakage. This process is regulated through complex interactions between VEGF and structural proteins in the endothelium that form the intercellular junctions between neighboring endothelial cells, VE-cadherin and β -catenin. Phosphorylation of these junctional proteins induces conformational changes in these molecules, with subsequent losses in cell–cell adhesion.² This in turn leads to a reduction in the vascular barrier that controls fluid movement from the blood compartment to the interstitium. The importance of kinases in regulating major cellular signaling events such as cell survival,^{3–6} cell migration,^{7–10} and transformation and apoptosis^{11–14} has long been recognized, and perturbation in these pathways has been implicated in a number of diseases including cancer and inflammation.^{15,16} The critical roles that kinases play in regulating the vascular barrier have been extensively researched.^{17–19} These studies suggest that the inhibition of the implicated signaling pathways might prove therapeutically effective for the treatment of diseases and injuries associated with microvascular barrier function such as ischemic conditions where edema accumulation is believed to contribute to tissue damage.

In the regulation of microvascular processes, two major signaling pathways, the Src family and the PI3K signaling cascade in endothelial cells (Figure 1), are of pivotal importance. A frequent target for intervention downstream of receptor

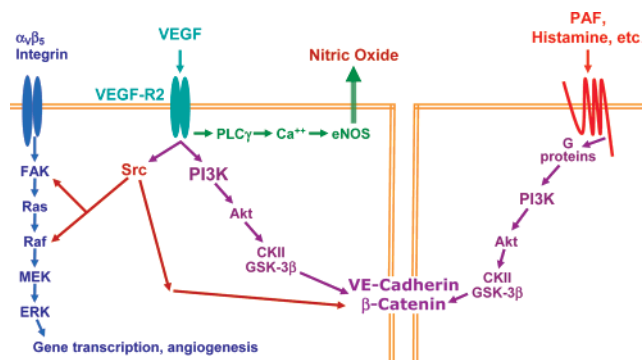


Figure 1. Kinase pathways regulating endothelial cell junction integrity. The two major signal transduction pathways in the regulation of intercellular integrity shown in this figure are Src and PI3K. PI3K can be activated via multiple growth factors or through G protein coupled PAFs. Signaling through Src can also affect gene transcription via ERK activation.

tyrosine kinases is Src,^{20–23} but investigations on PI3K inhibitors for a while was confined to natural products such as wortmannin, analogues of wortmannin,²⁴ semisynthetic viridine analogues, quercetin, LY294002 (a quercetin analogue), and staurosporin.^{25–27} Even though wortmannin is very potent inhibitor of PI3K, its development was hampered by its toxicity, insolubility, and aqueous instability. Several analogues of wortmannin were developed to circumvent these challenges. One such analogue is a pegylated wortmannin derivative, PWT-458, currently being developed by Wyeth Research.²⁸ This pegylation of wortmannin resulted in a compound with improved plasma stability and reduced toxicity. Studies with synthetic, small molecules have focused primarily on the catalytic domain and specifically the ATP binding site of these proteins. Several inhibitors of PI3K were reported recently including 1-benzopyran-4-ones,²⁹ benzoxazines,³⁰ benzothiophenes,³¹ tetrazole benzofurancarboxamides,³² pyrimidine carboxamides,³³ and fused azolepyrimidines.³⁴

* Author to whom correspondence should be addressed. Telephone: (858)-678-0760. Fax: (858)-678-0762. E-mail: Palanki@targegen.com.

[†] TargeGen Inc.

[‡] BioPredict.

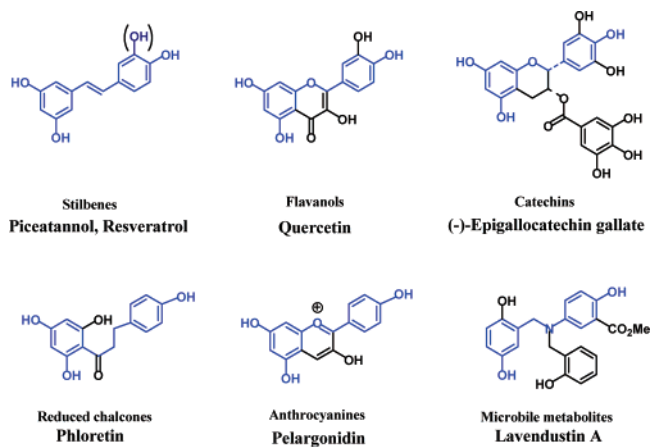
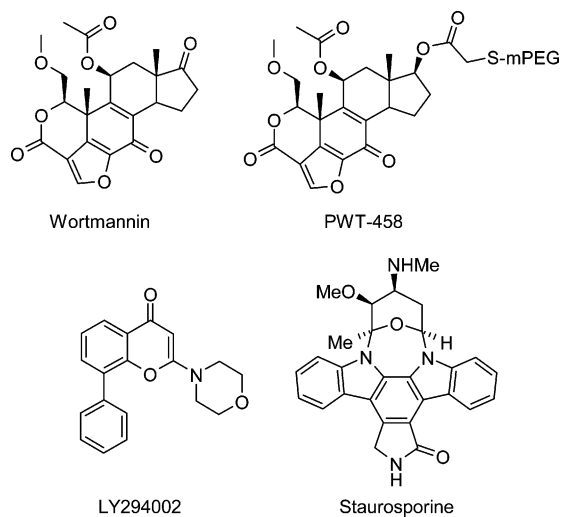


Figure 2. Six representative polyphenolic structures selected from different families and origins, all of which have a common motif shown in blue. The pharmacophore identified from these structures served as template for structural elaboration.

Thus, many drug design schemes have concentrated on heterocyclic ring structures mimicking the pyrimidine portion of ATP and being capable of affinity competition with ATP. In this paper we report for the first time the discovery of a highly selective and potent PI3K inhibitor, 6,7-bis(3-hydroxyphenyl)pteridine-2,4-diamine, and the evolution of this lead via structure–*in vivo* activity correlations. We discovered common structural motifs from natural products such as polyphenols, including flavonoids which are known to have vascular protective properties^{35–40} (Figure 2) and combined with ATP mimics to design new structural class of compounds for targeting PI3K. Another important aspect of the design involved the incorporation of a phenolic group in the inhibitor. In general, the phenolic group in a drug molecule is considered less desirable due to its ability to undergo Phase II metabolism and elimination. However, the rapid elimination of the drug from a body is a desirable property in developing compounds with acute interventions, where a short time window for action followed by rapid clearance may be desirable, as in the case of targeting myocardial infarction.

Our design concept was to incorporate ATP-like structures (aminopyrimidine or aminopyridine) into the natural product pharmacophore to generate novel hybrid molecules with the expectation of combining high affinity for the ATP binding site of kinases and high selectivity from a balance between the ATP-like and hydrophobic interactions of the new structures (Figure 3).

Functionalization through either the 2 and 4 position (X, Y) of the pyrimidine or pyridine and the 6 and 7 positions (R1, R2) (pteridine class) or 2 and 3 position (pyridopyrazine class) of the pyrazine ring (Figure 4) allowed for structural elaboration and enabled us to systematically generate structure–activity profiles.

In this paper we wish to communicate the results of this drug discovery effort to the point of lead selection and target verification. Preclinical myocardial infarct model studies and details of pharmacology were reported recently.⁵⁴

Design and Synthesis. The new pteridines were synthesized from substituted 5,6-diaminopyrimidines by condensation reactions with substituted phenylglyoxals or benzils. Reactions using phenylglyoxals were carried out under conditions which yielded regioselective isomers as shown in Scheme 1.

Condensation of 2,3-diamino- or 3,4-diaminopyridines with substituted benzils or phenylglyoxals affords 2,3-substituted pyrido[2,3-*b*]pyrazin-6-ylamines (Scheme 2) or 2,3-substituted pyrido[3,4-*b*]pyrazin-8-ylamines (Scheme 3).

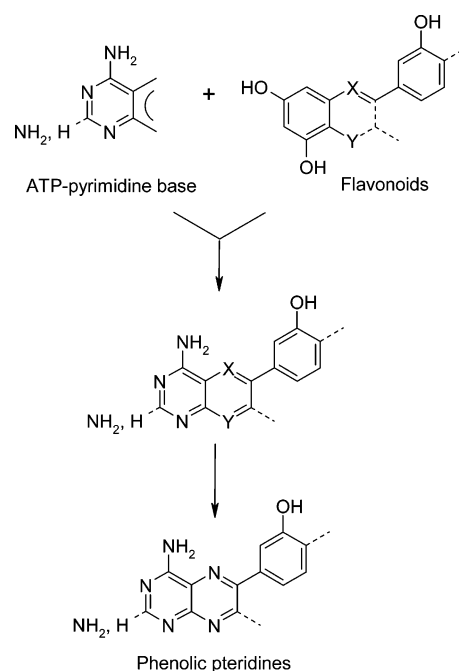


Figure 3. Evolution of an ATP-phenolic hybrid as an example for the design of pteridines incorporating the basic pharmacophore with the correct regioisomeric configuration.

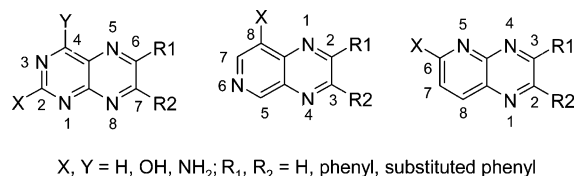
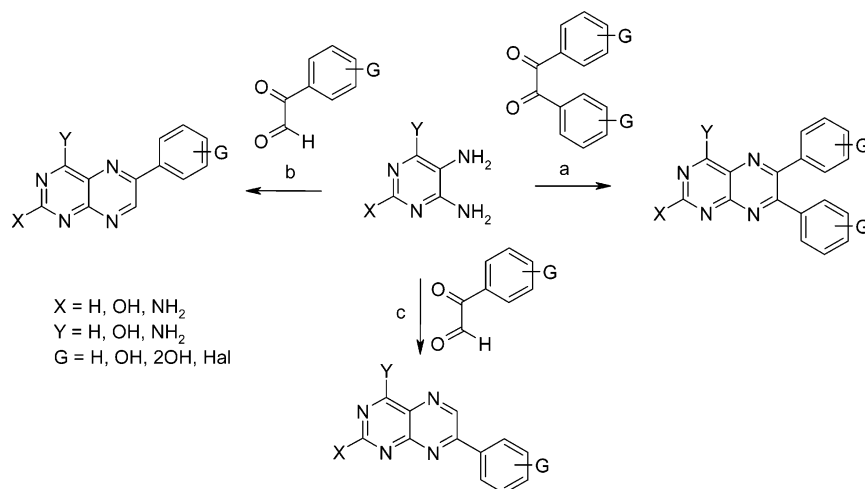


Figure 4. Pteridine and pyridopyrazine templates for structural elaboration.

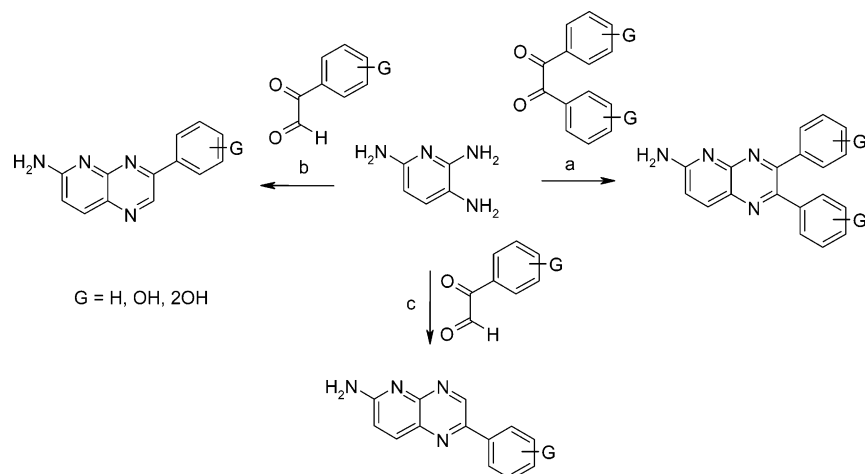
All benzils and glyoxals, with the exception of 3,3-dihydroxy- and 3,3',4,4'-tetrahydroxybenzils, 3',4'-dihydroxyphenylglyoxal, and 3-hydroxyphenylglyoxal were commercially available. Certain noncommercial glyoxals, 3,4,5-triaminopyridine,⁴¹ and 2,3,6-triaminopyridine⁴² were synthesized based on published procedures.

Results and Discussion

1. Synthesis. The synthetic strategy was based on a modular approach, starting with prefunctionalized intermediates with up

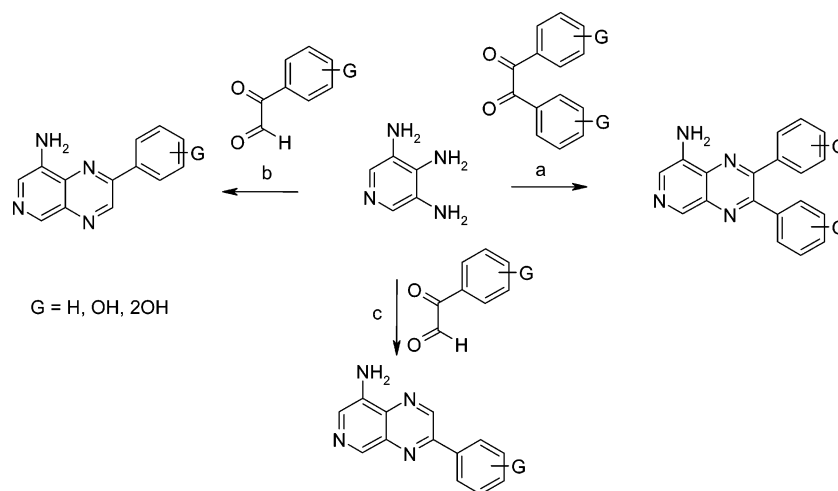
Scheme 1^a

^a (a) NaHCO₃, MeOH–water; (b) Me₂C=NOH, HCl, water, pH = 3–4; (c) NaOH, MeOH–water, pH = 9–10

Scheme 2^a

^a (a) NaHCO₃, MeOH–water; (b) NaOH, MeOH–water, pH = 9–10; (c) Me₂C=NOH, HCl, water, pH = 3–4.

Scheme 3

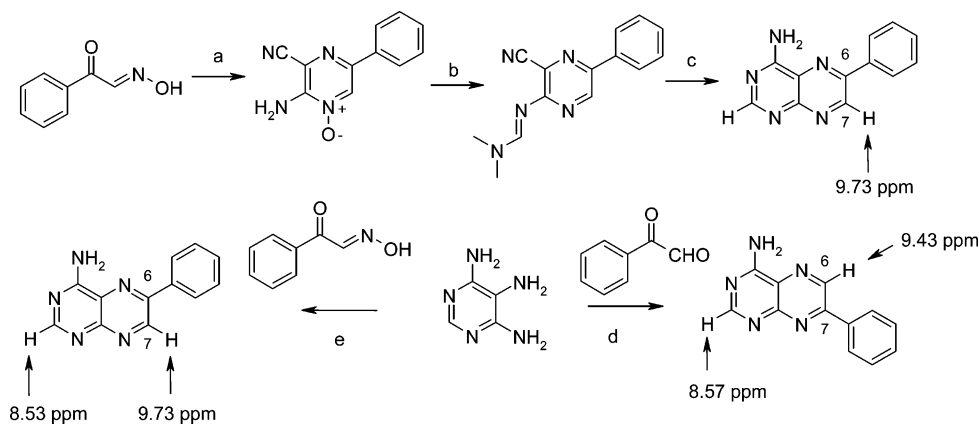


^a (a) NaHCO₃, MeOH–water; (b) NaOH, MeOH–water, pH = 9–10; (c) Me₂C=NOH, HCl, water, pH = 3–4.

to 14 positions available for structural elaborations. The cyclocondensation reaction of the aminosubstituted heterocycles with either substituted benzils or glyoxals forming the central pyrazine ring in a single step resulted in final products in nearly quantitative yields and in high purity. A large variety of substituted diaminopyrimidines, pyridines, benzils, and glyoxals

were commercially available for initial synthesis. However, several benzils and glyoxals are not commercially available and synthesized based on published procedures. Reaction conditions involving the condensation of *o*-diamines with glyoxals were developed to obtain either the 6- or 7-substituted regioisomers selectively. The ability to obtain regioisomers proved to be

Scheme 4



^a (a) $(\text{CN})_2\text{CHNH}_2 \cdot \text{TosOH}$, 2-propanol, Rt; (b) PCl_3 , $(\text{MeO})_2\text{CHNMe}_2$; (c) NH_4OAc , AcOH, reflux; (d) NaHCO_3 , 1:1 dioxane/water, pH ~ 9–10; (e) MeOH/H₂O, reflux. Analysis of intermediates with ¹H NMR in DMSO-*d*₆, 500 MHz Bruker NMR.

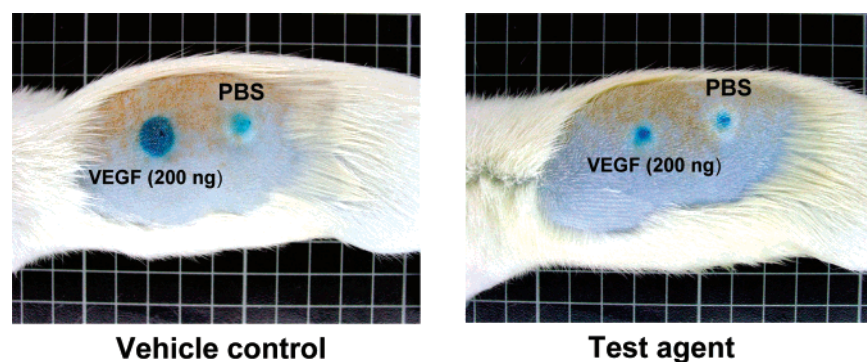


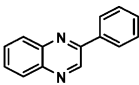
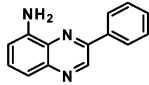
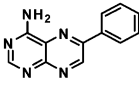
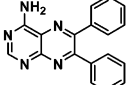
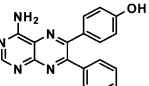
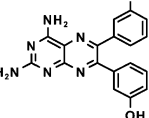
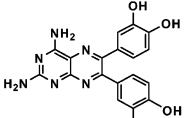
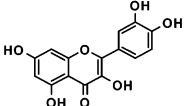
Figure 5. Miles assay for determining the inhibition of VEGF induced vascular permeability in Sprague–Dawley rats. (For details, see Experimental Section).

valuable during the biological screening phase of the project. Unequivocal preparation of 6-substituted pteridines unaccompanied by the 7-substituted isomer was first reported by Taylor et al.⁴³ Since then, the regioselective syntheses of 6- and 7-substituted pteridines have been reported by several groups.^{44,57} Generally, the regioselective synthesis of 6-substituted pteridines is achieved by condensation of 4,5,6-triamino- and 2,4,5,6-tetraaminopyrimidines with substituted phenylglyoxal monooximes in MeOH.^{45,57} 7-Substituted pteridines were previously reported via pH-controlled condensation of 2,4,5,6-tetraaminopyrimidine with substituted benzylglyoxals.⁴⁶ Above a pH of 8 only the 5-amino group of 2,4,5,6-tetraaminopyrimidine is nucleophilic enough to react with aldehyde groups of benzylglyoxals, thus resulting in 7-substituted pteridines. In the preparation of 6- and 7-substituted pteridines, we were interested in a rapid elucidation of the regioisomeric structure by ¹H NMR spectroscopy. Thus, the 4-amino-6-phenylpteridine, prepared by the unequivocal route reported by Taylor et al.,⁴³ was in all respects identical to the compound prepared by the condensation of 4,5,6-triaminopyrimidine with oximinoacetophenone in MeOH. A comparison of the ¹H NMR spectrum of 4-amino-7-phenylpteridine, prepared by the condensation of 4,5,6-triaminopyrimidine with phenylglyoxal, with the ¹H NMR spectrum of 4-amino-6-phenylpteridine showed that the C-7-H is shifted downfield to 9.73 ppm compared to C-6-H at 9.43 ppm. The C-2-H of 4-amino-6-phenylpteridine, however, is slightly shifted upfield to 8.54 ppm compared to C-2-H of 4-amino-7-phenylpteridine at 8.57 ppm, as shown in Scheme 4.

2. Lead Identification from *In Vivo* Screen. The occurrence of vascular permeability (VP) results from (1) edema from receptor tyrosine kinases such as VEGFR2⁴⁷ and G-protein

coupled receptors such as platelet-activating factor (PAF),⁴⁸ (2) hypoxia-inducible factor (HIF) induced upregulation of VEGF,⁴⁹ and (3) the influence of nitric oxide on vascular tone. A complex network of signal transduction pathways are triggered (Figure 1) by the activation of G protein coupled receptor using either VEGF, PAF, or histamine. This leads to the dissociation of a complex of intercellular junctional proteins and ultimately to a leaky endothelium. For the inhibition of VP, proteins other than growth factors and downstream kinases, for example the destabilization of HIF-1 α ⁵⁰ or nitric oxide synthase,^{51,57} have also been suggested as potential targets for developing new drugs. Given the complex nature and multiple targets likely to be involved in VP, we selected an *in vivo* screen, the Miles assay, instead of a biochemical kinase inhibition screen for initial structure–activity profiling.⁵⁸ This simple assay consists of injecting rats intravenously with test agent followed by intravenous injection of Evans blue. Evans blue binds to plasma proteins and thus allows for visual assessment of vascular leakage. The intradermal injection of VEGF on each flank produces a blue stain (Figure 5). On the basis of the area and intensity of this stain, we graded the edema at the intradermal injection site according to a 12 point scale and thus were able to test the ability of agents to inhibit vascular leakage directly. In each rat, the scores for both the right and left flank injection sites were summed to yield a composite score. A 4-point scale was utilized, where 3 = background response (bluing equivalent to intradermal saline controls), 2 = minimal bluing (surrounding area <25% intensity of injection site), 1 = midlevel bluing (surrounding area about 50% of intensity of injection site), and 0 = maximal bluing (surrounding area >75% of intensity of injection site). Scores for four reaction sites were summed to

Table 1. Inhibition of Vascular Permeability of a Selected Number of Pyrazines and Quercetin

Compound	Structure	Miles Score
1		0
2		0
3		2
4		5
5		7
6		10
7		11
Quercetin		3

produce a final score rating from 0 (maximal vascular permeability) to 12 (background edema response). Overall responses are ranked according to the following scale: score 0–4 = low to no activity, 5–8 = moderate activity, 9–12 = high activity. Results of a representative number of compounds tested this way are shown in Table 1.

We started with the simplest, nonfunctionalized phenylquinoline **1** which constituted the basic scaffold identified from our natural product search (Figure 2) and then systematically added structural complexity according to our design scheme in Figure 3. From the results of the Miles score it became immediately apparent that inhibition of vascular permeability in these heterocyclic compounds depended predominantly on the nature of substituents on both sides of the hybrid structures. For example, the change of structure from a quinoline **2** to a pteridine **3** was crucial in the development of inhibitory activity. Nearly maximum activity (score 10–11) as obtained for compounds **6** and **7**, which required extensive functionalization of both the heterocyclic ring structure and aromatic groups to the right of the pyrazine ring. Particularly, the presence of phenolic hydroxyls added substantially to increases in the potency of these pteridines. The flavonoid quercetin, tested as

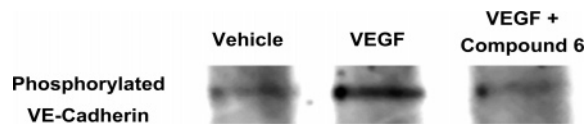


Figure 6. Western blot of lysates from VEGF-induced increase in VE-cadherin in HUVEC cells. The figure shows the prevention of VEGF-induced phosphorylation of VE-cadherin by compound **6**. Serum-starved HUVEC cells (Cambrex BioScience, Walkersville, MD) were treated for 15 min with compound **6** (0.125 to 10 μ M) or vehicle, followed by a 5-min treatment with 20 ng/mL recombinant VEGF (PeproTech, Rocky Hill, NJ) or vehicle. Cell pellets were suspended in RIPA buffer (10 to 1 v/v, Pierce) on ice for 10 min. The cell suspension was passed through a 23 gauge needle (3 \times) to complete the lysis process. Lysed cells were centrifuged at 16 000 rcf at 4 $^{\circ}$ C for 10 min. The supernatant was removed, and the protein was assayed using the BCA method (Pierce). After calculating protein concentration, RIPA buffer was added to adjust the concentration. Laemmli buffer (Pierce) was added to the samples and heated at 100 $^{\circ}$ C for 10 min. Samples were loaded onto an SDS polyacrylamide gel. Gels were probed with antibody specific for phosphorylated VE-cadherin. The antibody was removed and probed with the antibody for total VE-cadherin. The antibodies for both phosphorylated VE-cadherin and unphosphorylated VE-cadherin were purchased from Cell Signaling Technology, Inc. (Danvers, MA).

a control, also showed inhibition of vascular leak in this screen, although, as the score indicated, at a considerable lower level than the corresponding hybrid structures (**5**, **6**, and **7**). In summary, the *in vivo*–SAR studies identified basic structural elements in these molecules which are required for high inhibition (Miles score above 7) of vascular permeability. It was clearly shown that these novel hybrid molecules incorporating the aminopyrimidino or pyridinopyrazine scaffold in place of the chromenone-fused ring structure of flavonoids dramatically improved the potency. The selection of **6** as a lead compound was the result of this *in vivo* screen. In the following discussion, we present the data in support of identifying a molecular target and the cellular signaling path for the inhibitory activity of this lead compound.

3. Target–Path Verification of the Lead Compound.

Endothelial junctions are formed by transmembrane adhesion proteins. These include members of the claudin family, occludin, junctional adhesion molecules (JAM) A, B, and C, and endothelial cell selection adhesion molecules (ESAM). At adherens junctions, the main adhesion protein is VE-cadherin. Phosphorylation of VE-cadherin has been reported to regulate VEGF-induced changes in microvascular permeability⁵² in a manner that can be blocked by inhibitors of kinases such as Src family kinases.¹⁸ In order to evaluate the effect of compound **6** on this process, human umbilical vein endothelial cells (HUVEC) were exposed to the compound, and VE-cadherin was monitored by immunoprecipitation of cell lysates. The results of western blots are shown in Figure 6, where a VEGF-induced increase in total level of VE-cadherin was observed, and this process was inhibited by prior exposure of cells to 10 μ M of **6**. Before Western Blot analysis, protein concentrations in each well was measured using the bicinchoninic acid (BCA) method (using reagents from Pierce). Using the information obtained on amount of protein from each well, the gel loading was adjusted to ensure equal amounts of protein. β -Actin was used as second control to ensure that equal amount of protein was loaded on to the gel. The gel was probed with an antibody targeting phosphorylated VE-cadherin. Further, the antibody was removed, and the gel was probed with an antibody targeting VE-cadherin for analysis. On the basis of our experiments, we are confident that the compound is not degrading VE-cadherin protein but merely inhibiting phosphorylation of VE-cadherin.⁵³

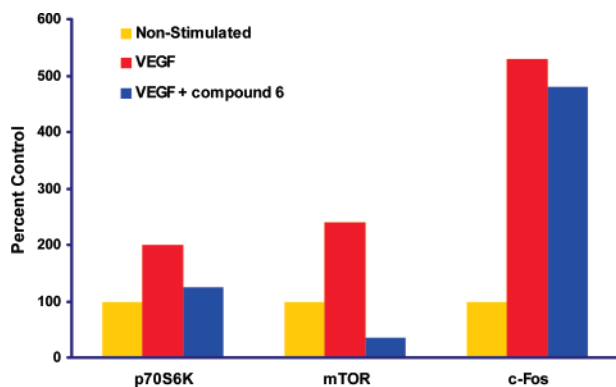


Figure 7. Selected results from the Kinexus screen of 73 kinase targets. The figure shows the inhibition of VEGF induced mTOR and p70s6S kinases in HUVEC cell lysates. While LY294002 and wortmannin inhibits c-Fos (data not shown), compound **6** does not. Basal activation of cell signaling proteins in HUVECs was first down-regulated by starving the cells for 4 h, followed by exposure to 20 ng/mL VEGF in the absence or presence of 10 mM **6** for 10 min. HUVECs were rinsed with ice-cold phosphate-buffered saline and then lysed by addition of RIPA buffer (100 mM Tris pH 7.5, 150 mM NaCl, 1 mM EDTA, 1% deoxycholic acid, 1% Triton X-100, 0.1% SDS, 2 mM PMSF, 500 mM NaF, 1 mM vanadate). Protein concentration was determined using the BCA method according to the manufacturer's instructions (Pierce, Rockford, IL). Cell lysates were adjusted to equivalent protein concentrations and then sent to Kinexus Bioinformatics for screening against four antibody panels representing 73 distinct phosphorylated kinases.

Only gel that is exposed to antibody targeting phosphorylated VE-cadherin is shown.

Cell lysates from this experiment were also used to determine phosphorylated ERK (data not shown). Treatment of the cells with VEGF stimulates VE-cadherin through the PI3K pathway and ERK through the Src pathway. The inhibitors targeting PI3K do not affect VEGF stimulated ERK pathway. Importantly we found that compound **6** does not affect this path, thus potentially avoiding inhibition of endothelial cell proliferation. The latter result was confirmed in cell culture, where no inhibition of endothelial cell proliferation was observed (data not shown).⁵⁴ Cell lysates prepared similarly to those of the previous assay were also confirmed via commercial screen (Kinexus Bioinformatics Co., Vancouver, BC, Canada) of 73 kinase targets.⁵⁵ Results from this screen show that compound **6** inhibited VEGF mediated phosphorylation of mTOR, p70S6 kinase as shown in Figure 7. Both p70S6K and mTOR are downstream of PI3K and were inhibited as expected. The biochemical profile of compound **6** contrasts with two commonly used PI3K targeting reagents, wortmannin and LY294002. This was confirmed by **6**'s inhibition of PI3K pathway signaling but (unlike wortmannin and LY294002) its sparing of ERK and cFos phosphorylation. One of the disadvantages of LY294002 and wortmannin is their effect on c-Fos which was inhibited by these two compounds (data not shown). C-Fos, a family of intermediate early genes, is present in many tissues in very low levels under basal conditions. C-Fos plays a dual role; in some cases their expression is protective to cells and involved in cellular proliferation, but they are also implicated in apoptosis.⁵⁶ It is beneficial to have a PI3K inhibitor that does not inhibit this key proto-oncogene.

The pathway data presented here established that **6** altered VEGF-mediated changes in phosphorylation but did not directly confirm what molecular targets it acts on to bring about these alterations. However, strong inhibition (80%) of mTOR phosphorylation suggested the PI3K/Akt path, since mTOR is directly phosphorylated by Akt. Figure 8 shows the inhibition

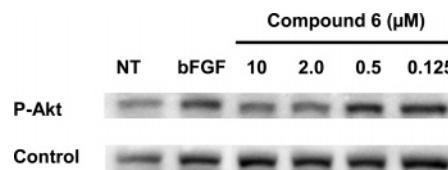


Figure 8. Western blots of lysates from FGF-stimulated HUVEC cells, where the inhibition of phosphorylation of Akt was observed in a dose-dependent manner. Serum-starved HUVECs (Cambrex BioScience, Walkersville, MD) were treated for 15 min with compound **6** (0.125 to 10 μ M) or vehicle, followed by a 5-min treatment with 20 ng/mL recombinant bFGF (PeproTech, Rocky Hill, NJ) or vehicle. Cell pellets were suspended in RIPA buffer (10 to 1 v/v, Pierce) on ice for 10 min. The cell suspension was passed through a 23 gauge needle (3 \times) to complete the lysis process. Lysed cells were centrifuged at 16 000 ref at 4 $^{\circ}$ C for 10 min. The supernatant was removed, and the protein was assayed using the BCA method (Pierce). After calculating protein concentration, RIPA buffer was added to adjust the concentration. Laemmli buffer (Pierce) was added to the samples and heated at 100 $^{\circ}$ C for 10 min. Samples were loaded to SDS polyacrylamide gel. Gels were probed with antibody specific for phosphorylated Akt. The antibody was removed and probed with the antibody for total Akt. Control lanes show unphosphorylated Akt. The antibodies for both phosphorylated Akt and unphosphorylated Akt were purchased from Cell Signaling Technology, Inc. (Danvers, MA).

Table 2. Inhibition of PI3K Isoforms of Compound **6** in a Commercial Screen of 140 Kinases

kinase	IC ₅₀ (nM)
PI3K α	1300
PI3K β	1200
PI3K δ	235
PI3K γ	83

of Akt by **6**, and an Akt loading control for comparison. We observed inhibition of Akt at the background level of the vehicle control at the highest concentration, following blot intensities in a dose dependent manner.

Direct measurements of PI3K inhibition by **6** were done in a biochemical assay, which showed in an ATP competitive mode an IC₅₀ value of 83 nM for the gamma isoform of this enzyme. This isoform has previously been shown to play a central role in relaying inflammatory signals in general and specifically been implicated in edemas.⁵⁹ Taken together the results of cell-based and biochemical analysis strongly support the inhibition of PI3K signaling as a primary mechanism of drug action. We also tested compound **6** in a commercial biochemical kinase screen. The results showed inhibitory activity for only 8 out of a panel of 140 kinases, demonstrating the high target selectivity of this compound.⁶⁰ Inhibition data for the 4 isoforms is shown in Table 2.

4. Structure–Activity Correlations. Further insights into the structural features necessary for PI3K inhibitor activity were obtained from SAR of a selected number of structurally related analogues. The results are shown in Tables 3, 4, and 5. Table 3 gives IC₅₀ values for derivatives **8–16** in which the hydrophobic phenolic region including the pyrazine core structure of **6** was unchanged, and only the pyrimidine/pyridine region of the molecule was modified. The nature of substituents in this part of the molecule proved to be very important for binding to PI3K. In general, the data shows that any structural deviation in this region from compound **6** results in a loss of binding activity up to 4 orders of magnitude. Substitution of hydroxyl for amino groups as in compounds **12** and **13** results in nearly complete loss of PI3K binding. One reason for this loss may be that these molecules tautomerize, and that the amide form which is expected to dominate in these molecules would exhibit incompatible hydrogen bond donor/acceptor geometry for

Table 3. Structure–Activity Correlations of Compounds 8–16

Compound		IC50 for PI3Ky (uM)
8		17
9		9
10		Inactive
11		Inactive
12		46
13		48
14		4
6		0.083
15		51
16		Inactive

binding at the ATP site. Either mono- or disubstitution of the primary amino groups with solubilizing moieties such as shown in the examples of structure **15** and **16** results in essentially inactive compounds. These relatively bulky side groups apparently cannot be accommodated in the space available at the ATP site, an observation which was confirmed from the modeling studies (see section 5). The elimination of one amino group as in structure **14** or both amino groups as in structure **9** results in a loss in binding of nearly 2 orders of magnitude. Thus, the data in Table 3 clearly shows that the triplet HB-donor–acceptor-donor motif in these compounds is utilized by these compounds in binding to PI3K.

Table 4 summarizes the results for the compounds **17–28**, in which the 2,4-diaminopyrimidine portion of **6** was kept constant, and only the right side of the core structure was

Table 4. Structure–Activity Correlations of Compounds 17–28

Compound		IC50 for PI3Ky (uM)
17		0.0399
6		0.083
7		0.273
18		0.195
19		1.2
20		2.7
21		3.0
22		4.7
23		5.9
24		8.5
25		12.6
26		32.7
27		Inactive
28		Inactive

modified. Several important structural correlations were observed. For example, comparison of the two regioisomers (**17** and **21**) showed the 6' and 7'-substituted isomer to give IC₅₀ value of 40 nM and 3000 nM, respectively, a nearly 2 order of magnitude difference. It is interesting to note that the model

Table 5. Structure–Activity Correlations of Compounds 29–35

Compound	Structure	IC ₅₀ for PI3K γ (uM)
29		0.968
30		Inactive
31		Inactive
32		Inactive
5		4.0
33		5.1
34		1.3

structures of natural products, which served as templates for our initial design (Figure 2), suggested a preferential 6' over a 7' substitution. Another important requirement for high affinity binding to PI3K was the presence of meta-substituted hydroxyl groups (see comparison of structure **17** with **19**, and **6** with **20**). In fact the compounds listed in this table can be categorized into two subclasses, 6'-substituted phenols with meta-substituted hydroxyl groups (compounds **17**, **6**, **7**, and **18**), which gave nanomolar IC₅₀ values, and compounds **19–28** with other phenol substitution patterns, which fall into the micromolar binding range. The introduction of the solubilizing groups on the *m*-hydroxyphenol moiety of compound **6** resulted in essentially inactive derivatives (**26–28**).

Table 5 shows SAR results for compounds **29–35**. A comparison of the IC₅₀ values of these compounds clearly confirms the importance of the second nitrogen in the pyrimidine ring in contributing to PI3K binding. Compounds **30**, **31**, and **32** and compounds **10** and **11** lacking a nitrogen in the second ring failed to exhibit any binding activity to PI3K, even if all other structural requirements for high affinity binding are fulfilled.

In summary, the structural requirements for high binding of pteridines to PI3K are (1) the presence of the 2,4-diaminopyrimidine moiety, (2) 6'-regioselectivity, and (3) *m*-hydroxyphenyl substitution in addition to requirement 2. The minimum structure which satisfies all three requirements is shown in compound **17**, which so far has also exhibited the best PI3K binding activity. It is interesting that the SAR profiles generated in Table 3, 4 and 5 correlate quite well with the results of the

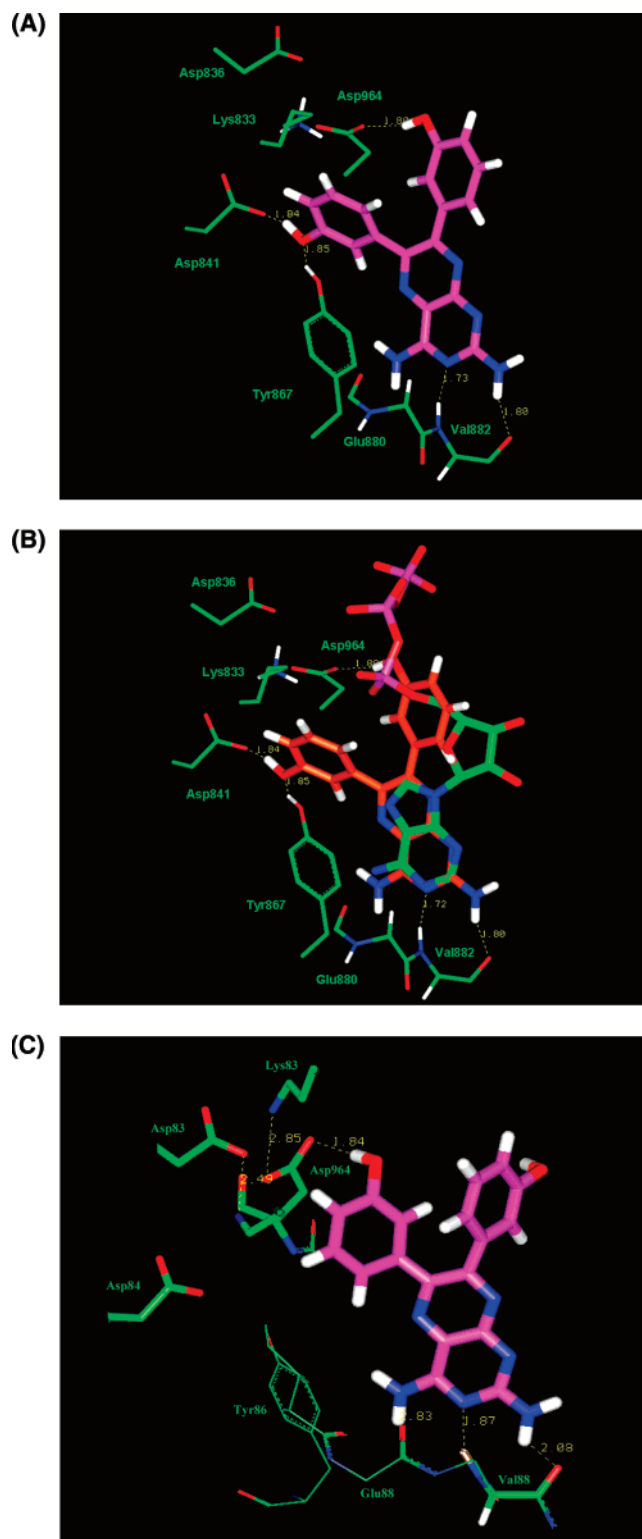
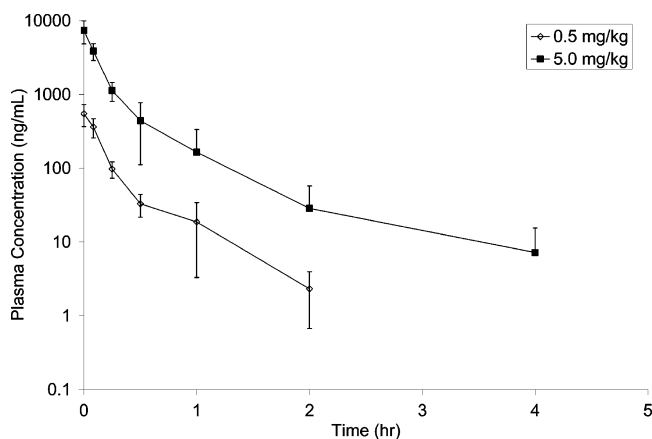


Figure 9. Model structures of the human PI3K γ kinase showing the location of compound **6** in the catalytic domain. (A) An expanded view of compound **6** in the ATP pocket of the enzyme, with specific interactions shown. (B) Compound **6** in the ATP binding site overlapped with ATP from 1E8X. Complexes were superimposed using a method due to Lesk⁶⁸ that superimposes corresponding carbon alpha atoms in residues near the ATP adenine ring. (C) Compound **6** docked in an alternative binding mode. Renderings in (A) through (C) were generated using the software package Insight II.

initial *in vivo* screen, further supporting the involvement of PI3K as a target for the inhibition of vascular permeability in these compounds.

Table 6. Mean Pharmacokinetic Parameters Following Intravenous Doses of **6** in Rats

dose (mg/kg)	C_0 ($\mu\text{g/mL}$)	C_{max} ($\mu\text{g/mL}$)	$\text{AUC}_{(0-\text{inf})}$ (h $\mu\text{g/mL}$)	$t_{1/2}$ (hr)	CL (mL/min/kg)	Vd_{ss} (L/kg)
0.5	0.713 ± 0.266	0.363 ± 0.105	0.124 ± 0.033	0.4 ± 0.1	71 ± 20	2.3 ± 0.7
5.0	7.73 ± 2.53	3.33 ± 0.44	1.38 ± 0.56	0.8 ± 0.3	66 ± 23	4.4 ± 0.5

**Figure 10.** Mean plasma concentration–time profiles following intravenous doses of **6** in rats.

5. Molecular Modeling. The SAR data was used together with molecular models of the interaction between compound **6** and PI3K to gain insights into how it might inhibit this kinase. Compound **6** was docked into the active site of the enzyme [1E8Z] using a combination of interactive modeling using the Insight II program⁶¹ and automated docking software.⁶² The resulting complex was then minimized in the molecular mechanics program DISCOVER using the CFF force field with a distance-dependent dielectric.⁶¹ In optimizing the complex, all atoms were allowed to move in residues with at least one atom within 8 Å of any atom of the ligand. The modeling experiments suggest a mode of binding that is summarized in Figures 9a through 9c. Two strong hydrogen bonds are formed from the ligand to the backbone of the protein in the hinge region of PI3K γ : the first is from the N-3 nitrogen of the pteridine ring serving as an acceptor to the backbone NH of Val 882 and the second is from 4-primary amine group serving as a donor to the backbone carbonyl of the same residue (Figure 9a). While the second NH₂ group on compound **6** is positioned adjacent to the backbone carbonyl of Glu 880, the geometry for formation of a hydrogen bond is poor. For reference, ATP from the ATP/PI3K γ (*Sus scrofa*) complex in 1E8X is shown overlaid on the model in Figure 9b. The pattern of hydrogen bonds observed in 1E8X to the backbone is similar, with a strong hydrogen bond formed to the NH of Val 882 and a second potential hydrogen bond to the backbone carbonyl of Glu 880 either geometrically weak or absent. A pocket is evident at the back of the ATP binding site that accommodates the 6'-substituted *m*-phenol of compound **6** (Figure 9c). Asp 841, on the $\alpha 3$ helix, lies at the back of this pocket and can form a hydrogen bond with the OH group of the 6'-substituted *m*-phenol. Additional stabilization of the phenolic group can come from the side chain of Tyr 867, which can swing to assist in the coordination. The second phenolic group can form an interaction with the side chain of Asp 964 that is part of the DFG loop.

Overall the modeling data is consistent with nearly all of the SAR profiling results in Table 4. Using the first binding mode (Figure 9a), one can see that both phenolic groups are involved in the hydrogen bond. The first binding mode also explains the activity of both compounds **6** and **17**. However, the second

binding mode (Figure 9c) shows only one phenolic group is involved in hydrogen bonding and not the other. Both binding modes explain the SAR results. Based on the modeling work on this series, it appears that the binding mode depicted in Figure 9a provides better explanation of the data.

6. Pharmacokinetic Studies in Rats. The *in vivo* pharmacological work using compound **6** was completed in rats and shown below. We also completed the pharmacodynamic work using compound **6** using Sprague–Dawley rats.⁵⁴ In order to fully elucidate the properties of **6**, the pharmacokinetic (PK) parameters of **6** were studied in Sprague–Dawley rats following intravenous administration of either 0.5 or 5.0 mg/kg. The mean intravenous PK parameters for **6** in the rat are presented in Table 6. After single intravenous administration, **6** displayed an approximate first-order decline in plasma concentrations with respect to time (Figure 10). Using a noncompartmental model, the intravenous plasma pharmacokinetics of **6** at doses of either 0.5 or 5.0 mg/kg were characterized by high clearance (CL approximately equal to hepatic blood flow), a moderate volume of distribution (3-fold to 6-fold total body water), and a short plasma half-life ($t_{1/2}$) ranging from 0.4 h to 0.8 h. Dose-proportional pharmacokinetic parameters were observed following doses of 0.5 to 5.0 mg/kg. A 10-fold increase in dose resulted in a 10-fold increase in plasma exposure parameters (C_0 , C_{max} , and AUC_{inf}).

7. Summary. Starting from a natural product search of vasoprotective agents with kinase inhibitory activities, we identified a pharmacophore useful for the design of novel hybrid molecules which incorporated structures mimicking the ATP binding motif for competitive inhibition. The synthesis of an initial set of compounds followed by SAR profiling in an *in vivo* screen identified a lead, **6**, for clinical development. Pathway analysis identified this lead as a potent and selective inhibitor of PI3K. Structural reiteration, combined with molecular modeling studies, elucidated the molecular details necessary for high affinity binding and validated both our initial hybrid design concept and *in vivo* targeting approach.

The biochemical profile of compound **6** contrasts with two commonly used PI3K inhibitors, wortmannin (an equipotent but pan-isoform inhibitor) and LY294002 (a weak inhibitor). These distinctions suggest the three compounds should differently influence cellular processes. This was confirmed by **6**'s inhibition of PI3K pathway signaling but (unlike wortmannin and LY294002) its sparing of ERK and c-Fos phosphorylation. Additionally **6** had no influence on mitogenesis whereas the other compounds inhibited cell proliferation and even survival. Wortmannin's effects might arise from its inhibition of PI3K α and/or β . Alternatively this may represent off-target hits, as wortmannin inhibits MAP kinase, myosin light chain kinase, and mTOR in the sub- μM range.⁶⁵ LY294002's cytotoxicity likely reflects off-target hits such as Raf or GSK3 β inhibition,⁶⁶ or non-PI3K-dependent pro-apoptotic effects mediated via intracellular H₂O₂.⁶⁷ Of most relevance to cardioprotection, however, is that **6** inhibited VEGF-induced pro-inflammatory events (VE-cadherin phosphorylation) while sparing those that control mitogenesis. VEGF plays both positive (pro-angiogenic) and negative (pro-edema) roles in I/R injury, and differentiating between these processes would be beneficial in a proposed MI therapy.

Several PI3K inhibitors are currently in development as antitumor drugs. However, the role of PI3K in myocardial infarction was not fully exploited for drug discovery efforts. A biphasic I/R injury to the heart is caused by myocardial infarction. Despite a great understanding of the cause, very little progress has been made in this area due to the fact that an antiischemia therapy is required early in MI pathogenesis, a time when the great majority of patients are inaccessible. There is a large body of evidence suggesting that PI3K is an attractive target for developing compounds for ischemia. Several commonly known PI3K inhibitors reduce inflammatory events in animal models but fail to reduce infarct size when delivered after reperfusion. We have developed a PI3K γ/δ inhibitor to interrupt the reperfusion phase of I/R injury, that shows reduced infarct development and improved myocardial function.⁵⁴ Compound **6** also offered cardioprotection upon delivery up to several hours after reperfusion.⁵⁴ On the basis of this promising profile in models of leakage and ischemia reperfusion injury, **6** (TG100-115) has been selected for clinical development.⁶³

Experimental Section

Miles Assay. Experiments were conducted according to NIH Guidelines for the use of laboratory animals. Non-fasted male Sprague–Dawley rats (Harlan, Indianapolis, IN), weighing between 175 and 200 g, were injected via tail vein with either vehicle or 200 μ L of test compound (from 10 mM stock formulations). Treatment groups sizes were $N = 2-4$. Two hours posttreatment, rats were anesthetized with ip injection and placed on a heating pad set to 35–37 °C. Evans blue dye (500 μ L of a 2% saline, 0.2 μ m sterile filtered) was administered iv. Immediately following dye injections, animals received two intradermal injections of VEGF (200 ng total) in a volume of 100 μ L. Thirty minutes after this challenge, vascular permeability was visually assessed by the extent of Evans blue tattooing at the injection sites. Agonist injection sites were scored based on the degree of extravasation into the surrounding dermis and compared to the neighboring PBS injection site. In each rat, the scores for both the right and left flank injection sites were summed to yield a composite score. A 4-point scale was utilized, where 3 = background response (bluing equivalent to intradermal saline controls), 2 = minimal bluing (surrounding area <25% intensity of injection site), 1 = midlevel bluing (surrounding area about 50% of intensity of injection site) and 0 = maximal bluing (surrounding area >75% of intensity of injection site). Scores for four reaction sites were summed to produce a final score rating from 0 (maximal vascular permeability) to 12 (background edema response). Overall responses are ranked according to the following scale: score 0–4 = low to no activity, 5–8 = moderate activity, 9–12 = high activity.

Determination of PI3K Activity. For the determination of IC₅₀ values of the compounds shown in Table 3, 4, and 5, we used a luminescence-based kinase assay with recombinant phosphatidylinositol 3-kinase- p-120 gamma, alpha, beta, and delta (Upstate Cell Signaling Solutions). In white, flat-bottom, 96-well plates (Nunc) parallel assays were run at ambient temperature at final volumes of 50 μ L. Each well contained 40 μ L of buffer consisting of 20 mM Tris buffer, pH 7.4, containing 4 mM MgCl₂, 10 mM NaCl, 50 μ M d-*myo*-phosphatidylinositol-4,5-bisphosphate substrate (Echelon Bioscience, Inc.) and an appropriate amount of PI3K (250–500 ng/well). The final concentration of compound in these experiments ranged from 100 to 0.001 μ M and was done by direct addition of compound in 2.5 μ L of DMSO. Then 10 μ L of ATP was added to the wells from a stock of 3 μ M. After 90 min, 50 μ L of Kinase-Glo reagent (Promega) was added to terminate the reaction, and the well content was allowed to equilibrate for an additional 10 min. Luminosity was measured using an Ultra 384 instrument (Teca). IC₅₀ values were calculated from the luminescence–concentration curves using the nonlinear curve fitting capabilities of Prism (Version4, GraphPad software).

Preparation of Cell Lysates. Cell lysates were produced from human umbilical vein endothelial cells (HUVEC, Cambrex, Bioscience, Walkersville, MD) between passage 2 and 4 by incubation for 4 h with serum free medium (EBM-2 medium Cambrex BioScience) in order to downregulate basal activation of cell signaling proteins. This was followed by exposure for 10 min of 20 ng/mL recombinant human VEGF (catalog no. 100-20 Pepro-Tech, Rocky Hill, NJ) in the absence or presence of compound **6** (10 μ M in dimethyl sulfoxide) into EBM-2 medium. HUVEC cells were then rinsed with ice cold PBS by the addition of 300 μ L RIPA buffer (100 mM Tris pH 7.5, 150 mM NaCl, 1 mM EDTA, 1% deoxycholic acid, 1% Triton X-100, 0.1% SDS, 2 mM PMSF, 500 mM NaF, 1 mM vanadate). Protein concentrations were determined using the bicinchoninic acid method according to the manufactures instructions (Pierce, Chemical, Rockford, IL). These lysates were used in various cell-based assays. Cell lysates were adjusted to equivalent protein concentrations and then sent to Kinexus Bioinformatics (Kinexus Bioinformatics Corp., Vancouver, British Columbia, Canada) for screening against four antibody panels representing 73 distinct phosphorylated kinases, which analyses cell lysates using a Western-blot-based protocol in order to identify phosphorylated signaling proteins in a quantitative manner.

K_i Value Determination. The K_i value for **6** was determined against PI3-kinase (p120 γ) using a fluorescence polarization-based assay. Briefly, assays were run at room temperature and a final volume of 50 μ L containing buffer, an appropriate amount of the PI3K such that the assay was linear over 60 min, and varying amounts of ATP in the presence of a fixed varied amount of **6**. The reaction was initiated by the addition of PIP₂ at a final concentration of 50 μ M. After the reaction was allowed to proceed for 60 min, fluorescence polarization reagent was added to terminate the kinase reaction and then allowed to proceed for an additional 10 min to maximize the signal. Control reactions containing no ATP were used for each varied ATP concentration. Enzyme reaction rates were derived by calculating the difference between kinase catalyzed and noncatalyzed reactions at a specific **6** concentration. The K_i value was derived from rate data using competitive enzyme kinetics curve fitting. On the basis of the data analysis of curve fitting, the compound was judged to be an ATP-competitive inhibitor.

Molecular Modeling. Modeling studies were conducted in collaboration with BioPredict Inc., Oradell NJ. Protein coordinates for human PI3K γ were taken from the PDB entry 1E8Z, a cocrystal of human PI3K γ @ 2.4 Å with staurosporin. Additional structures of human and *Sus scrofa* PI3K γ available from the PDB were superimposed to examine potential protein flexibility and modes of binding to other ligands (1E7U, 1E7V, 1E8W, and 1E8Y). *Sus scrofa* PI3K γ is 95% identical in sequence to human PI3K γ ; all residues within 8 Å of staurosporin in 1E8Z are identical.

Pharmacokinetic Studies of 6. All animals were housed separately and had continual access to food and water. All doses were administered as aqueous solutions containing 9.5% Captisol (Cydrex). Heparinized whole blood samples were obtained and centrifuged to separate plasma, and the plasma was stored at –70 °C until bioanalysis. Male Sprague–Dawley rats, body weight 200 to 250 g, from Charles River, received an intravenous **6** bolus dose of either 0.5 or 5 mg/kg into the tail. Serial plasma samples were isolated from rats ($N = 5$ animals per dose route) over the following time course: 5, 15, and 30 min and 1, 2, 4, 6, 8, and 24 h. Blood samples (0.25 mL) were isolated through an indwelling jugular vein catheter. Plasma samples were extracted by addition of a 2-fold excess of acetonitrile containing internal standard followed by centrifugation. The supernatants were isolated for analysis. Processed plasma samples were quantitated by LC/MS/MS against external calibration standards prepared in blank rat plasma. The performance of each analytical run was assessed by quality control samples prepared in plasma matrix. The standard calibration curves ranged from 1 to 10 000 ng/mL. The LC/MS/MS system consisted of an Sciex API4000 triple quadrupole mass spectrometer (MDS Sciex), an Agilent 1100 HPLC system (Agilent Technologies, Inc), and a CTC autosampler (Leap Technologies).

The LC separations were performed on a Waters Xterra, C₁₈, 15 × 2.1 mm, 2.5 μm reverse phase HPLC column (Waters Corporation). The column temperature was kept at 60 °C. Mobile phase A consisted of 1.0% formic acid (FA) in water and mobile phase B consisted of 1.0% FA in acetonitrile. The flow rate was kept constant at 0.5 mL/min. Following a 20 μL sample injection, mobile B was held at 5% for 0.5 min followed by a linear increase to 95% mobile phase B over 1.6 min. The mass spectrometric detection of **6** and internal standard was achieved using electrospray ionization operating in positive ionization mode. The molecular ion transitions were monitored in MRM mode. The maximum plasma concentrations following intravenous dosing (C₀) were extrapolated from the apparent distribution phase for individual animals. Plasma clearance (CL) was calculated as dose/AUC_(0–inf) while the volume of distribution at steady state (Vd_{ss}) was calculated as CL × MRT, where MRT (mean residence time) was defined as AUMC_(0–inf)/AUC_(0–inf). The area under the curve, AUC_(0–inf), from individual concentration data were calculated using the linear trapezoidal rule.

Chemistry. All solvents and reagents were obtained from commercial sources and used without further purification. 3,3'-Dihydroxybenzil, 4,4'-dihydroxybenzil, and 3,3',4,4'-tetrahydroxybenzil, 3-hydroxyphenylglyoxal hydrate, and 4-hydroxyphenylglyoxal hydrate were purchased from Midori Kagaku Co Ltd. ¹H nuclear magnetic resonance (NMR) spectra were recorded on a 500 MHz Bruker NMR. Chemical shifts are reported in parts per million (δ) downfield from the tetramethylsilane resonance in the indicated solvent. Coupling constants are reported in hertz (Hz). Mass spectra were obtained from a Waters LC/MS spectrometer. This system includes a 2795 separation module, a 996 photodiode array detector and a ZQ2000 mass spectrometer. A Zorbax SB column (150 × 4.6 mm 3.5 μm, Agilent Technologies) is used for the LC. Column temperature is 40 °C. Compounds are separated using gradient elution with mobile phases of water (0.05% TFA (A)) and acetonitrile (0.05% TFA (B)). The mass spectrometer is equipped with an electrospray probe. Source temperature is 120 °C. All of the compounds were identified using the positive mode with mass scan range from 100 to 800. Elemental analyses were performed at NuMega Laboratories (San Diego) on a Perkin-Elmer Series II – 2400 CHNS analyzer, and the results are within 0.4% of the calculated values unless otherwise stated.

6-Phenylpteridin-4-amine (3). Ammonium acetate (192.7 mg, 2.5 mmol) was suspended in 3 mL of glacial acetic acid, and the mixture was heated to ca. 100 °C. *N*-(3-cyano-5-phenylpyrazin-2-yl)-*N,N*-dimethylimidiformamide (125.6 mg, 0.5 mmol) was added, and the reaction mixture was refluxed for 1 h. Then it was cooled down to ambient temperature, and solvent was removed *in vacuo*. The resulting residue was washed once with 10 mL of methanol and twice with 40 mL of diethyl ether and dried *in vacuo* to give the product as a light-yellow solid. ¹H NMR (DMSO-*d*₆): δ 7.55–7.60 (m, 3 H), 8.31 (br s, 1 H), 8.46 (br s, 1 H), 8.49 (dd, *J*₁ = 8.2 Hz, *J*₂ = 1.9 Hz, 2 H), 8.54 (s, 1 H), 9.73 (s, 1 H).

6,7-Diphenylpteridin-4-amine (4) was prepared according to the literature.⁴²

4,4'-(4-Aminopteridine-6,7-diyl)diphenol (5). 4,5,6-Triaminopyrimidine sulfate (2.23 g, 10.0 mmol) was added in small portions to a solution of sodium bicarbonate (1.68 g, 20.0 mmol) in 50 mL of DI water with vigorous stirring. A brisk evolution of CO₂ gas was observed. The resulting suspension was heated to 80 °C, and 4,4'-dihydroxybenzil (2.42 g, 10.0 mmol) was added to the mixture. The reaction mixture was refluxed for 3 h, at which point a light-yellow precipitate was formed in abundance. The precipitate was filtered, washed sequentially with water (2 × 40 mL), methanol (1 × 20 mL), and diethyl ether (2 × 40 mL) and dried *in vacuo* to give 3.14 g of the title product (93.3% yield) as light-yellow solid. 95.5% purity by LC/MS (230 DAD). MS *m/z* [MH⁺] = 332.8. ¹H NMR (DMSO-*d*₆) δ 6.72–6.73 (d, *J* = 8.7 Hz, 2H), 6.74–6.75 (d, *J* = 8.7 Hz, 2H), 7.35–7.37 (d, *J* = 8.6 Hz, 2H), 8.40–7.42 (d, *J* = 8.6 Hz, 2H), 8.06 (br s, 1H), 8.15 (br s, 1H), 8.50 (1H, s), 9.77 (br s, 1H), 9.87 (br s, 1H). Anal. (C₁₈H₁₃N₅O₂·0.1H₂O) C, H, N.

3,3'-(2,4-Diaminopteridine-6,7-diyl)diphenol (6). 2,4,5,6-Tetraaminopyrimidine sulfate (4.76 g, 20.0 mmol) was added in small portions to a solution of sodium bicarbonate (3.36 g, 40.0 mmol) in 100 mL of water with vigorous stirring. A brisk evolution of CO₂ gas was observed. The resulting suspension was heated to 80 °C and 3,3'-dihydroxybenzil (4.84 g, 20.0 mmol) was added to the mixture. The reaction mixture was refluxed for 3 h, at which point a bright-yellow precipitate was formed in abundance. The precipitate was filtered, washed sequentially with water, methanol, and diethyl ether and dried *in vacuo* to give 6.46 g (93.3% yield) of the title product as bright-yellow solid, 98.10% purity by LC/MS (230 DAD). MS *m/z* [M + H⁺] = 347.7. ¹H NMR (DMSO-*d*₆) δ 6.75–6.77 (dd, *J*₁ = 8.2 Hz, *J*₂ = 2.0, 1H), 6.79–6.80 (dd, *J*₁ = 8.2 Hz, *J*₂ = 2.0, 1H), 6.81–6.83 (d, *J* = 7.8 Hz, 2H), 6.86–6.87 (d, *J* = 7.8 Hz, 2H), 6.93 (s, 1H), 6.97 (s, 1H), 7.08–7.10 (t, *J* = 7.8 Hz, 1H), 7.09–7.11 (t, *J* = 7.8 Hz, 1H), 7.75 (br s, 1H), 8.02 (br s, 1H), 9.56 (br s, 2H). ¹³C NMR (DMSO-*d*₆) δ 115.2, 116.1, 116.5, 116.6, 120.5, 120.5, 120.6, 129.0, 129.0, 140.1, 140.3, 145.4, 154.3, 157.0, 157.1, 157.6, 163.0, 163.3. Anal. (C₁₈H₁₄N₆O₂) C, H, N.

4,4'-(2,4-Diaminopteridine-6,7-diyl)dibenzene-1,2-diol (7): 96.5% yield of the product as yellow, fluffy powder. 97% purity by LC/MS (230 DAD). MS *m/z* [MH⁺] = 379.3. ¹H NMR (MeOH-*d*₄) δ 6.68–6.70 (d, *J* = 8.1 Hz, 1H), 6.71–6.73 (d, *J* = 8.1 Hz, 1H), 6.79–6.81 (dd, *J*₁ = 8.1 Hz, *J*₂ = 2.1 Hz, 1H), 6.84–6.86 (dd, *J*₁ = 8.1 Hz, *J*₂ = 2.0 Hz, 1H), 6.93 (d, *J* = 2.0 Hz, 1H), 7.03 (d, *J* = 2.1 Hz, 1H). ¹H NMR (DMSO-*d*₆) δ 6.47 (br s, 2H), 6.57–6.59 (d, *J* = 8.1 Hz, 1H), 6.59–6.61 (d, *J* = 8.6 Hz, 1H), 6.64–6.66 (dd, *J*₁ = 8.1 Hz, *J*₂ = 1.8 Hz, 1H), 6.65–6.67 (dd, *J*₁ = 8.6 Hz, *J*₂ = 1.8 Hz, 1H), 6.90–6.91 (d, *J* = 1.8 Hz, 1H), 6.95 (d, *J* = 1.8 Hz, 1H), 7.41 (br s, 2H).

3,3'-(6-Aminoquinaxoline-2,3-diyl)diphenol Hydrochloride Salt (8). 1,2,4-benzenetriamine dihydrochloride (40.4 mg, 0.206 mmol) and 3,3'-dihydroxybenzil (50.0 mg, 0.20 mmol) were dissolved in 2 mL of 1:1 mixture of dioxane–water. The reaction was refluxed for 3 h. Then solvent was removed *in vacuo*. The residue was dissolved in 2 mL of methanol, and this solution was added dropwise to 40 mL of diethyl ether with stirring. The formed dark-red precipitate was collected, washed with diethyl ether and dried *in vacuo* to give the title compound **8** (69.8 mg, 85.4% yield) as red solid, 97.6% purity by LC/MS (230 DAD). MS *m/z* [MH⁺] = 330.8. ¹H NMR (MeOH-*d*₄) δ 6.81–6.83 (dd, *J*₁ = 8.0 Hz, *J*₂ = 1.8 Hz, 1H), 6.85–6.87 (dd, *J*₁ = 8.0 Hz, *J*₂ = 1.2 Hz, 1H), 6.96–6.98 (m, 3H), 6.98 (d, *J* = 1.8 Hz, 1H), 7.10 (d, *J* = 2.3 Hz, 1H), 7.13–7.16 (t, *J* = 8.0 Hz, 1H), 7.28–7.31 (t, *J* = 8.0 Hz, 1H), 7.56–7.58 (dd, *J*₁ = 9.5 Hz, *J*₂ = 2.3 Hz, 1H), 8.04–8.06 (d, *J* = 9.5 Hz, 1H). ¹H NMR (DMSO-*d*₆) δ 5.9 (br s, 3H), 6.74–6.77 (m, 2H), 6.83–6.86 (m, 2H), 6.92–6.93 (t, *J* = 2.0 Hz, 1H), 6.97–6.98 (t, *J* = 2.0 Hz, 1H), 7.07–7.10 (t, *J* = 7.9 Hz, 1H), 7.15–7.18 (t, *J* = 7.9 Hz, 1H), 7.31 (d, *J* = 1.7 Hz, 1H), 7.51–7.54 (dd, *J*₁ = 9.1 Hz, *J*₂ = 2.4 Hz, 1H), 7.97–7.99 (d, *J* = 9.1 Hz, 1H). Anal. (C₂₀H₁₅N₃O₂·HCl·1.7H₂O) C, H, N.

3,3'-Pteridine-6,7-diyl diphenol (9). A 5 mL reaction vial equipped with a stirring vane was charged with 4,5-diaminopyrimidine (110 mg, 1.00 mmol, 1.00 equiv), 3,3'-dihydroxybenzil (242 mg, 0.500 mmol, 1.00 equiv), and *m*-cresol (0.750 mL). The slurry was heated to ca. 200 °C and within 10 min gave rise to a dark colored solution. A dull orange precipitate started to form in ca. 20 min and remained through the rest of the heating. The reaction was cooled to room temperature and was triturated by pouring into diethyl ether (30 mL) to yield a dark green precipitate. The solid was isolated and washed with 3 × 30 mL of diethyl ether and dried *in vacuo* to yield the title compound as a 1/1 complex with *m*-cresol (341 mg). MS *m/z* [MH⁺] = 365.1. ¹H NMR (DMSO-*d*₆) δ 6.88–6.90 (m, 4H), 6.95 (app t, *J* = 8.0 Hz, 2H), 7.05 (dd, *J*₁ = 2.0 Hz, *J*₂ = 2.0 Hz, 1H), 7.14 (dd, *J*₁ = 2.0 Hz, *J*₂ = 2.0 Hz, 1H), 7.17–7.22 (q, *J* = 7.9 Hz, 2H), 8.73 (d, *J* = 7.3 Hz, 1H), 9.46 (s, 1H), 9.67 (br s, 1H), 9.71 (br s, 1H).

3,3'-(8-Aminopyrido[3,4-*b*]pyrazine-2,3-diyl)diphenol Hydrochloride Salt (10). 3,4,5-Triaminopyridine dihydrochloride (60.0 mg, 0.304 mmol) and 3,3'-hydroxybenzil (99.6 mg, 0.41 mmol)

were heated at 190 °C in 1.0 mL of *m*-cresol for 1 h. Then the mixture was cooled down to ambient temperature and mixed thoroughly with 35 mL of diethyl ether. The formed brown precipitate was collected, washed repeatedly with diethyl ether, and dried *in vacuo* to give the title compound **10** (93.9 mg, 78.4% yield) as greenish-brown powder. MS *m/z* [MH⁺] = 331.4. ¹H NMR (MeOH-*d*₄) δ 6.88–6.91 (m, 2H), 6.99–7.01 (m, 1H), 7.07–7.10 (m, 2H), 7.13–7.14 (t, *J* = 2.1 Hz, 1H), 7.18–7.22 (dt, *J*₁ = 8.0 Hz, *J*₂ = 3.6 Hz, 2H), 8.03 (s, 1H), 8.82 (s, 1H). ¹H NMR (DMSO-*d*₆) δ 6.85–6.87 (m, 3H), 6.98–7.01 (m, 1H), 7.02–7.03 (t, *J* = 2.0 Hz, 1H), 7.09–7.10 (t, *J* = 2.0 Hz, 1H), 7.14–7.16 (t, *J* = 7.9 Hz, 1H), 7.15–7.17 (t, *J* = 7.9 Hz, 1H), 8.08 (d, *J* = 0.74 Hz, 1H), 8.94 (d, *J* = 0.74 Hz, 1H), 9.78 (br s, 2H). Anal. (C₁₉H₁₄N₄O₂·HCl·1.5H₂O) C, H, N.

3,3'-(6-Aminopyrido[2,3-*b*]pyrazine-2,3-diyl)diphenol Hydrochloride Salt (11). 2,3,6-Triaminopyrimidine dihydrochloride (197.0 mg, 1.0 mmol) and 3,3'-dihydroxybenzil (242.4 mg, 1.0 mmol) were dissolved in 3.0 mL of 1:1 mixture of dioxane–water. The reaction mixture was refluxed for 3 h, and then solvent was removed *in vacuo*. The resulting greenish solid was dissolved in 3 mL of MeOH, and this solution was added to 40 mL of diethyl ether with vigorous stirring. The formed precipitate was collected, washed with diethyl ether, and dried *in vacuo* to give 342.9 mg (90.4% yield) of the product as light-green powder, 99.0% purity by LC/MS (230 DAD). MS *m/z* [MH⁺] = 331.8. ¹H NMR (MeOH-*d*₄) δ 6.83–6.85 (m, 2H), 6.88–6.90 (m, 1H), 6.95–6.97 (m, 2H), 7.02–7.03 (t, *J* = 1.9 Hz, 1H), 7.14–7.17 (t, *J* = 8.0 Hz, 1H), 7.15–7.18 (t, *J* = 7.8 Hz, 1H), 7.36–7.38 (d, *J* = 9.5 Hz, 1H), 8.43–8.46 (d, *J* = 9.5 Hz, 1H). ¹H NMR (DMSO-*d*₆) δ 6.76–6.80 (m, 4H), 6.91–6.92 (t, *J* = 2.0 Hz, 1H), 6.98–6.99 (t, *J* = 2.0 Hz, 1H), 7.11–7.14 (t, *J* = 7.8 Hz, 1H), 7.12–7.15 (t, *J* = 7.8 Hz, 1H), 7.46–7.48 (d, *J* = 9.5 Hz, 1H), 8.43–8.45 (d, *J* = 9.5 Hz, 1H), 8.83 (br s, 1H), 9.71 (br s, 1H), 9.90 (br s, 1H). Anal. (C₁₉H₁₄N₄O₂·0.6HCl·1.5H₂O) C, H, N.

6,7-Bis(3-hydroxyphenyl)pteridine-2,4-diol (12). 5,6-Diamino-2,4-dihydroxypyrimidine sulfate (240.1 mg, 1.0 mmol) was suspended in 25 mL of DI water, and solid sodium bicarbonate (168.0 mg, 2.0 mmol) was added to this suspension. The reaction mixture was stirred at ambient temperature for 15 min. Then a solution of 3,3'-dihydroxybenzil (242.4 mg, 1.0 mmol) in 10 mL of methanol was added. The reaction mixture was brought to reflux and refluxed for 3 h. At this point it formed an orange solution with a yellow precipitate. The reaction mixture was cooled down to ambient temperature, and the resulting precipitate was centrifuged down and washed sequentially with 2 × 40 mL of DI water, 1 × 10 mL of MeOH, and 2 × 40 mL of diethyl ether and dried *in vacuo* to give 220.2 mg of the title compound as light-yellow fluffy solid, 63.2% yield, 99.3% purity by LC/MS (230 DAD). MS *m/z* [MH⁺] = 349.0. ¹H NMR (DMSO-*d*₆) δ 6.68–6.70 (d, *J* = 7.9 Hz, 1H), 6.72–6.74 (dd, *J*₁ = 7.9 Hz, *J*₂ = 1.6 Hz, 1H), 6.77–6.80 (m, 2H), 6.88 (t, *J* = 1.1 Hz, 2H), 7.08–7.11 (t, *J* = 7.9 Hz, 1H), 7.11–7.13 (t, *J* = 7.9 Hz, 1H), 9.52 (br s, 1H), 9.60 (br s, 1H), 11.66 (br s, 1H), 11.97 (br s, 1H). Anal. (C₁₈H₁₂N₄O₄·H₂O) C, H, N.

2-Amino-6,7-bis(3-hydroxyphenyl)pteridin-4-ol (13). 6-Hydroxy-2,4,5-triaminopyrimidine sulfate (239.2 mg, 1.0 mmol) was suspended in 25 mL of DI water, and solid sodium bicarbonate (168.0 mg, 2.0 mmol) was added to this suspension. The reaction mixture was stirred at ambient temperature for 15 min. Then a solution of 3,3'-dihydroxybenzil (242.4 mg, 1.0 mmol) in 10 mL of methanol was added. The reaction mixture was brought to reflux and refluxed for 3 h. At this point it formed a yellow solution with a yellow precipitate. The reaction mixture was cooled down to ambient temperature, and the resulting precipitate was centrifuged down and washed sequentially with 2 × 40 mL of DI water, 1 × 10 mL of MeOH, and 2 × 40 mL of diethyl ether and dried *in vacuo* to give 231.2 mg of the title compound **13** as reddish-yellow solid, 66.5% yield, 99.1% purity by LC/MS (230 DAD). MS *m/z* [MH⁺] = 348.0. ¹H NMR (DMSO-*d*₆) δ 6.68–6.70 (d, *J* = 7.9 Hz, 1H), 6.69–6.72 (dd, *J*₁ = 7.9 Hz, *J*₂ = 2.0 Hz, 1H), 6.75–6.77 (dd, *J*₁ = 7.9 Hz, *J*₂ = 2.4 Hz, 1H), 6.77–6.79 (d, *J* = 7.9 Hz, 1H), 6.88 (t, *J* = 2.0 Hz, 1H), 6.90 (t, *J* = 2.0 Hz, 1H), 7.05–

7.09 (t, *J* = 7.9 Hz, 1H), 7.09–7.12 (t, *J* = 7.9 Hz, 1H), 6.95 (br s, 2H), 9.47 (br s, 1H), 9.52 (br s, 1H), 11.50 (br s, 1H). Anal. (C₁₈H₁₂N₄O₄·0.9H₂O) C, H, N.

3,3'-(4-Aminopteridine-6,7-diyl)diphenol (14). 4,5,6-Triaminopyrimidine sulfate (2.23 g, 10.0 mmol) was added in small portions to a solution of sodium bicarbonate (1.68 g, 20.0 mmol) in 50 mL of water with vigorous stirring. A brisk evolution of CO₂ gas was observed. The resulting suspension was heated to 80 °C, and 3,3'-dihydroxybenzil (2.42 g, 10.0 mmol) was added to the mixture. The reaction mixture was refluxed for 1 h, during which time the starting materials completely dissolved and the product precipitated out as a light-yellow solid. The precipitate was collected, washed with water and then with methanol followed by diethyl ether, and dried *in vacuo* to give 3.14 g of the title product **14** (94.8% yield) as light-yellow solid, 100% purity by LC/MS (230 DAD). MS *m/z* [MH⁺] = 332. ¹H NMR (DMSO-*d*₆) δ 6.80–6.83 (m, 2H), 6.84–6.86 (d, *J* = 7.8 Hz, 1H), 6.93–6.94 (d, *J* = 7.8 Hz, 1H), 7.01–7.03 (m, 2H), 7.11–7.14 (dt, *J*₁ = 7.8 Hz, *J*₂ = 1.9 Hz, 2H), 8.23 (br s, 1H), 8.30 (br s, 1H), 8.59 (s, 1H), 9.63 (br s, 2H). Anal. (C₁₈H₁₃N₅O₂·0.55H₂O) C, H, N.

3,3'-(2-Amino-4-[(3-morpholin-4-ylpropyl)amino]pteridine-6,7-diyl)diphenol Trifluoroacetic Acid Salt (15). 3,3'-(2,4-Diaminopteridine-6,7-diyl)diphenol (1.0 g, 2.88 mmol) was dissolved in 5 mL of 4-(3-aminopropyl)morpholine, and sulfamic acid (0.530 g, 5.45 mmol) was added to this solution. The reaction mixture was refluxed for 18 h (ca. 160 °C). Then it was cooled down to ambient temperature, filtered through 0.22 μm syringe filter, and purified by reverse-phase preparative HPLC using a gradient of acetonitrile/water mixture with 0.1% of TFA. Fractions, containing the product, were collected. Solvent was removed *in vacuo* to afford 33.0 mg of the title product **15** as a brown viscous oil. MS *m/z* [MH⁺] = 474.5. ¹H NMR (DMSO-*d*₆) δ 3.07 (m, 2H), 3.20 (m, 2H), 3.44 (m, 2H), 3.59–3.80 (m, 6H), 3.97 (m, 2H), 6.78–6.85 (m, 4H), 6.91–6.92 (m, 2H), 7.13–7.17 (t, *J* = 7.9 Hz, 1H), 7.14–7.18 (t, *J* = 7.9 Hz, 1H).

3,3'-(2,4-Bis[(3-morpholin-4-ylpropyl)amino]pteridine-6,7-diyl)diphenol Trifluoroacetic Acid Salt (16). 3,3'-(2,4-Diaminopteridine-6,7-diyl)diphenol (1.0 g, 2.88 mmol) was dissolved in 5 mL of 4-(3-aminopropyl)morpholine, and sulfamic acid (0.530 g, 5.45 mmol) was added to this solution. The reaction mixture was refluxed for 18 h (ca. 160 °C). Then it was cooled down to ambient temperature, filtered through 0.22 μm syringe filter, and purified by reverse-phase preparative HPLC using gradient of acetonitrile/water mixture with 0.1% of TFA. Fractions, containing the product, were collected. Solvent was removed *in vacuo* to afford 800 mg of the title product **16** as a brown viscous oil. MS *m/z* [MH⁺] = 601.6. ¹H NMR (DMSO-*d*₆): δ 3.07 (m, 4H), 3.19 (m, 4H), 3.42 (m, 4H), 3.59–3.80 (m, 12H), 3.97 (m, 4H), 6.75–6.84 (m, 4H), 6.90 (m, 2H), 7.13–7.18 (m, 2H).

3-(2,4-Diaminopteridin-6-yl)phenol (17). 3-Hydroxyphenylglyoxal (2.1 g, 12.48 mmol) was dissolved in 100 mL of DI water. Acetone oxime (0.912 g, 12.48 mmol) was added, followed by 3 drops of 1 N aqueous hydrochloric acid to bring the pH to ca. 2–3. This solution was stirred at 50 °C for 1 h, 2,4,5,6-tetraaminopyrimidine sulfate (2.67 g, 11.23 mmol) was added, and the reaction mixture was stirred at ambient temperature for 3 h and refluxed for 6 h. At this point it formed a thick yellow suspension. The reaction was allowed to cool down to ambient temperature. Saturated aqueous sodium bicarbonate was added dropwise to bring the pH to ca. 6–7. The precipitate was collected, washed extensively with water, with 60 mL of methanol, and repeatedly with diethyl ether, and dried *in vacuo* to give 2.75 g of the title compound **17** (96.5% yield) as light-yellow solid. 99.5% purity by LC/MS (230 DAD). MS *m/z* [MH⁺] = 254.9. ¹H NMR (DMSO-*d*₆) δ 6.88–6.90 (dd, *J*₁ = 7.9 Hz, *J*₂ = 2.3 Hz, 1H), 7.16 (br s, 2H), 7.29–7.32 (t, *J* = 7.9 Hz, 1H), 7.66–7.67 (m, 1H), 7.72–7.73 (d, *J* = 7.9 Hz, 1H), 8.21 (br s, 1H), 8.27 (br s, 1H), 9.28 (s, 1H), 9.63 (s, 1H). Anal. (C₁₂H₁₀N₆O·1.7H₂O) C, H, N.

4-(2,4-Diaminopteridin-6-yl)benzene-1,2-diol (18). The same synthetic procedure as for compound **19**, 97.1% purity (97.5:2.5 ratio of regioisomers) by LC/MS (230 DAD). ELSD purity is 100%.

MS m/z $[MH^+] = 271.6$. 1H NMR (DMSO- d_6) for major regioisomer δ 6.85–6.88 (d, $J = 8.34$ Hz, 1H), 7.03 (br s, 2H), 7.61–7.63 (dd, $J_1 = 7.9$ Hz, $J_2 = 2.1$ Hz, 1H), 7.68 (d, $J = 2.1$ Hz, 1H), 8.18 (br s, 2H), 8.98 (s, 1H), 9.20 (s, 1H), 9.51 (s, 1H).

4-(2,4-Diaminopteridin-6-yl)phenol (19). A 10-mL reaction vessel equipped with a stirring bar and a reflux condenser was charged with 3-hydroxyphenylglyoxal (37.5 mg, 0.27 mmol; 1.00 equiv) was dissolved in 5 mL of methanol. Hydroxylamine hydrochloride (20 mg, 0.29 mmol) was added. This solution was stirred at 50 °C for 15 min, 2,4,5,6-tetraaminopyrimidine sulfate (60 mg; 0.25 mmol) was added, and the reaction mixture was heated to reflux for 3 h. The reaction was cooled, and a yellow precipitate started to form. The solution was neutralized using $NaHCO_3$ (satd, aqueous) to bring the pH to ca. 7. The solution was filtered, washed with water (1×30 mL), then with methanol (1×30 mL) and finally with ether (1×30 mL) and dried in the air, followed by vacuum to give the title compound **19** (32.0 mg, 50% yield) as a yellow solid, 100% purity by LC/MS (230 DAD), 100% purity by ELSD. $[MH^+] = 255.1$. 1H NMR (DMSO- d_6) δ 6.90 (d, $J = 1H$), 6.88 (d, $J = 8.5$ Hz, 2H), 7.62 (br s, 1H), 7.79 (br s, 1H), 8.15 (d, $J = 8.5$ Hz, 2H), 9.24 (s, 1H), 9.79 (s, 1H).

4,4'-(2,4-Diaminopteridine-6,7-diyl)diphenol (20). Same procedure as for compound **6**, 96.5% purity by LC/MS (230 DAD). MS m/z $[MH^+] = 347.7$. 1H NMR (DMSO- d_6): δ 6.58 (br s, 2H), 6.67–6.69 (d, $J = 8.8$ Hz, 2H), 6.69–6.72 (d, $J = 8.8$ Hz, 2H), 7.27–7.31 (m, 4H), 7.55 (br s, 1H), 7.64 (br s, 1H), 9.61 (s, 1H), 9.77 (s, 1H). Anal. ($C_{18}H_{14}N_6O_2 \cdot 2.2H_2O$) C, H, N.

3-(2,4-Diaminopteridin-7-yl)phenol (21). 2,4,5,6-Tetraaminopyrimidine sulfate (476.4 mg, 2.0 mmol) was suspended in 10 mL of DI water, and 7.5 M aqueous sodium hydroxide was added until the measured pH was ca. 9–10. Then 3-hydroxyphenylglyoxal (336.3 mg, 2.0 mmol) was added. The reaction mixture was stirred at ambient temperature for 3 h and then brought to reflux and refluxed for 3 h. At this point it formed a thick yellow suspension. The reaction was allowed to cool down to ambient temperature and 1 N aqueous hydrochloric acid was added dropwise to bring the pH to ca. 6–7. The precipitate was collected, washed extensively with water, with 60 mL of methanol, and repeatedly with diethyl ether and dried *in vacuo* to give the title compound **21** (469.3 mg, 92.3% yield) as a bright-yellow solid, 98.5% purity by LC/MS (230 DAD). MS m/z $[MH^+] = 254.9$. 1H NMR (DMSO- d_6) δ 6.83 (br s, 2H), 6.93–6.96 (dd, $J_1 = 8.0$ Hz, $J_2 = 2.1$ Hz, 1H), 7.33–7.36 (t, $J = 7.9$ Hz, 1H), 7.62–7.63 (m, 1H), 7.65 (d, $J = 0.83$ Hz, 1H), 7.83 (br s, 1H), 7.87 (br s, 1H), 8.85 (s, 1H), 9.77 (br s, 1H). Anal. ($C_{12}H_{10}N_6O \cdot 1.4H_2O$) C, H, N.

4-(2,4-Diaminopteridin-7-yl)phenol (22). This compound is made by stirring a 1:1 ratio of 4-hydroxyphenylglyoxal with the free base of the 2,4,5,6-tetraaminopyrimidine in water at a pH of 7 for ca. 3 h. The product is isolated by filtering the precipitated free base, washing sequentially with water (2×40 mL), methanol (1×40 mL), and ether (2×40 mL), and drying in vacuum desiccator. 1H NMR (DMSO- d_6): δ 6.57 (br s, 2H), 6.91 (d, $J = 8.5$ Hz, 2H), 7.55 (br s, 1H), 7.62 (br s, 1H), 8.09 (d, $J = 8.5$ Hz, 2H), 8.81 (s, 1H), 10.0 (br s, 1H).

4-(2,4-Diaminopteridin-7-yl)benzene-1,2-diol (23). This compound is made by stirring a 1:1 ratio of 3,4-dihydroxyphenylglyoxal with the free base of 2,4,5,6-tetraaminopyrimidine in water at a pH of 7 for ca. 3 h. The product is isolated by filtering the precipitated free base, washing sequentially with water (2×40 mL), methanol (1×40 mL), and ether (2×40 mL), and drying in a vacuum desiccator. 1H NMR (500 MHz; DMSO- d_6): δ 6.52 (br s, 2H), 6.84 (d, $J = 8.3$ Hz, 1H), 7.53 (dd, $J_1 = 8.3$ Hz, $J_2 = 2.1$ Hz, 1H), 7.53–7.56 (br s, 2H), 7.64 (d, $J = 2.3$ Hz, 1H), 8.71 (s, 1H).

6,7-Diphenylpteridine-2,4-diamine (24) was prepared according to literature.⁴² 97.5% purity by LC/MS (230 DAD). MS m/z $[MH^+] = 315.6$. 1H NMR (DMSO- d_6): δ 6.72 (br s, 2H), 7.28–7.44 (m, 10H), 7.69 (br s, 1H), 7.75 (br s, 1H).

6,7-Bis(3-methoxyphenyl)pteridine-2,4-diamine (25). A 5 mL reaction vial equipped with a stirring vane was charged with 2,4,5,6-tetraaminopyrimidine sulfate (119 mg, 0.50 mmol, 1.0 equiv), 3,3'-

dimethoxybenzil (135 mg, 0.50 mmol, 1.0 equiv), and *m*-cresol (1.0 mL). The slurry was heated to ca. 200 °C and within 10 min gave rise to a dark-green solution. A dull green precipitate started to form in ca. 20 min and remained through the rest of the heating. The reaction was cooled to room temperature and triturated by pouring into diethyl ether (30 mL) to yield a dull green precipitate. The solid was isolated and washed with 3×30 mL of diethyl ether and dried *in vacuo* to yield the title compound as green solid as a 1/1 complex with *m*-cresol (210 mg). The solid obtained as the sulfate salt as a complex with *m*-cresol (133 mg; 0.281 mmol; 1.0 equiv) was suspended in methanol (15 mL) in a reaction vessel equipped with a stirring bar. Amberlite chloride resin (GFS Chemical; 3.2 g) was added to the suspension. The resulting green-brown suspension was stirred at ca. 40 °C for 4 h, cooled to room temperature, filtered to remove the resin, and concentrated to yield an olive green solid. The solid was taken in ca. 4 mL of methanol and precipitated by adding into 40 mL of ether. The precipitate was washed with ether (2×40 mL) and dried in the air and then *in vacuo* to yield the title compound **25** as a grayish-green solid (58 mg, 55% yield), 100% purity by LC/MS (230 DAD), 98.4% purity by ELSD. MS m/z $[MH^+] = 375.5$. 1H NMR (DMSO- d_6) δ 3.64 (s, 3H), 3.67 (s, 3H), 6.93–6.98 (m, 2H), 6.98–6.99 (m, 3H), 7.10–7.12 (m, 1H), 7.23 (t, $J = 8.5$ Hz, 1H), 7.29 (t, $J = 8.0$ Hz, 1H), 7.70 (br s, 1H), 8.68 (br s, 1H), 9.20 (br s, 1H), 9.28 (br s, 1H).

3,3'-[(2,4-Diaminopteridine-6,7-diyl)bis(3,1-phenyleneoxy)]dipropene-1,2-diol Trifluoroacetic Acid Salt (26). To a solution of solketal (524 μ L, 4.2 mmol), triphenylphosphine (1.10 g, 4.2 mmol), and diisopropyl azodicarboxylate (DIAD, 827 μ L, 4.2 mmol) in 5 mL of anhydrous THF was added a solution of 3,3'-dihydroxybenzil (485 mg, 2.0 mmol) in 5 mL of anhydrous THF. The mixture was stirred at room temperature for 12 h. The solvent was removed, and the crude product was purified by silica gel column chromatography ($R_f = 0.8$, $CH_2Cl_2/MeOH$, 95:5) to give 1,2-bis[3-(2,2-dimethyl- 1,3 dioxolan-4-ylmethoxy)phenyl]ethane-1,2-dione as a yellow solid (378 mg, 40%). To a solution of 2,4,5,6-tetraaminopyrimidine sulfate (238 mg, 1.0 mmol) and sodium bicarbonate (168 mg, 2.0 mmol) in 5 mL water was added a solution of 1,2-bis[3-(2,2-dimethyl- 1,3 dioxolan-4-ylmethoxy)phenyl]ethane-1,2-dione (350 mg, 0.74 mmol) in 3 mL of methanol. The mixture was heated to 60 °C for 18 h, cooled to room temperature, and acidified with 1 N HCl to pH = 3. It was stirred at room temperature for 3 h, the solvent was removed, and the crude product was purified by preparative, reverse phase HPLC to give trifluoroacetate salt of the title compound **26** as a yellow solid (92.4 mg, 15%), 97.4% purity by LC/MS (230 DAD). MS m/z $[MH^+] = 495.5$. 1H NMR (MeOH- d_4): δ 3.61–3.65 (m, 4H), 3.83–3.98 (m, 6H), 7.01–7.06 (m, 3H), 7.09–7.12 (m, 3H), 7.24–7.27 (m, 2H).

6,7-Bis{3-[2-(diethylamino)ethoxy]phenyl}pteridine-2,4-diamine (27). A solution of 2-diethylaminoethyl chloride hydrochloride (1.03 g, 6.0 mmol), Cs_2CO_3 (3.9 g, 12 mmol), and 3,3'-dihydroxybenzil (727 mg, 3.0 mmol) in 30 mL of acetone was heated to reflux for 1.5 h and then cooled to ambient temperature. The solvent was removed *in vacuo*, and the crude product was purified by silica gel column chromatography ($R_f = 0.2$, MeOH/ Et_3N , 95.5:0.5) to give 1,2-bis[3-(2-diethylaminoethoxy)phenyl]ethane-1,2-dione as a yellow solid (823 mg, 62%). To a suspension of 2,4,5,6-tetraaminopyrimidine sulfate (434 mg, 1.82 mmol) and sodium bicarbonate (306 mg, 3.64 mmol) in 4 mL of water and 1 mL of 1,4-dioxane was added a solution of 1,2-bis[3-(2-diethylaminoethoxy)phenyl]ethane-1,2-dione (802 mg, 1.82 mmol) in 4 mL of methanol. The mixture was heated to reflux for 10 h, and then solvent was removed *in vacuo*. The crude product was purified by reverse phase preparative HPLC to give trifluoroacetate salt of the title product **27** as yellow solid (848 mg, 71%), 100% purity by LC/MS (230 DAD). MS m/z $[MH^+] = 545.6$. 1H NMR (MeOH- d_4): δ 1.34–1.38 (t, $J = 7.4$ Hz, 12H), 3.31–3.34 (q, $J = 7.4$ Hz, 8H), 3.58–3.60 (t, $J = 4.8$ Hz, 4H), 4.28–4.33 (dt, $J_1 = 11.6$ Hz, $J_2 = 4.8$ Hz, 4H), 7.09–7.13 (m, 4H), 7.23–7.24 (m, 2H), 7.27–7.30 (m, 2H).

(2,4-Diaminopteridine-6,7-diyl)di-3,1-phenylene Tetraethyl Bis(phosphate) (28). A 50-mL one-necked round-bottomed flask with a stirring bar and a septum was charged with 3,3'-dihydroxybenzil (512 mg; 2.11 mmol; 1.00 equiv) and acetonitrile (10 mL). To this partially dissolved mixture were added triethylamine (1.06 g; 14.9 mmol; 7.06 equiv), dimethylaminopyridine (DMAP) (506 mg; 4.13 mmol; 1.96 equiv), and dichloromethane (DCM, 10 mL) as cosolvents. Diethyl chlorophosphate (1.05 g; 6.09 mmol; 2.88 equiv) was added via a pipet over ca. 30 s. A white precipitate immediately formed and remained through the course of the reaction in the yellow solution. The reaction mixture was stirred for 3 d at room temperature after which it was concentrated by rotary evaporation to yield an off-white slurry. This oily slurry was partitioned between sodium bicarbonate (satd aqueous) and DCM. The aqueous layer was rewashed with 2 × 5 mL DCM, followed by extraction of the combined organics with 10 mL of 1 M HCl (aqueous). The combined organic layer was dried over anhydrous MgSO₄, filtered, and concentrated by rotary evaporation to yield the desired bis-phosphate ester material as light yellow slightly viscous oil. The compound does not require any purification but is easily purified by column chromatography using DCM–EtOAc (1:1) if needed. The chromatographically purified material is a yellow oil (911 mg; 89%). ¹H NMR (500 MHz; DMSO-*d*₆): δ 8.01 (d, *J* = 8.6 Hz, 4 H), 7.45 (d, *J* = 8.5 Hz, 4 H), 4.18–4.21 (m, 8 H), 1.28 (app t, *J* = 5.0 Hz, 12 H). A 60-mL reaction vessel with a stirring bar was charged with 2,4,5,6-tetraaminopyrimidine sulfate (188 mg; 0.791 mmol; 1.0 equiv) and sodium bicarbonate (10 mL solution containing 134 mg; 0.80 mmol; 1.01 equiv). The solution was heterogeneous at this point. After 10 min, the bis(phosphate) ester (499 mg; 0.971 mmol; 1.23 equiv) was added as a solution in methanol (9 mL). The solution was heated to ca. 60 °C and appeared turbid and yellow. The reaction was monitored to completion by HPLC in ca. 3 h time. The reaction mixture was cooled to room temperature and concentrated by rotary evaporation. The resulting yellow solid was dissolved in methanol, precipitated into ether, washed with 3 × 30 mL ether, and dried in the air, followed by drying *in vacuo*, resulting in the title compound **28** as a light yellow solid (0.20 g; 41%), 96.5% purity by LC/MS (230 DAD), 98.4% purity by ELSD. MS *m/z* [MH⁺] = 619.4. ¹H NMR (DMSO-*d*₆) δ 1.21–1.25 (m, 12H), 4.06–4.11 (m, 8H), 7.23–7.26 (m, 2H), 7.30–7.34 (m, 4H), 7.34–7.43 (m, 2H).

4,4'-[4-Aminopteridine-6,7-diyl]dibenzene-1,2-diol (29). Same procedure as for compound **6**. MS *m/z* [MH⁺] = 364.8. ¹H NMR (MeOH-*d*₄) δ 6.70–6.72 (d, *J* = 8.1 Hz, 1H), 6.73–6.75 (d, *J* = 8.1 Hz, 1H), 6.91–6.93 (dd, *J*₁ = 8.1 Hz, *J*₂ = 2.18 Hz, 1H), 6.93–6.95 (dd, *J*₁ = 8.1 Hz, *J*₂ = 2.18 Hz, 1H), 7.03 (d, *J* = 2.18 Hz, 1H), 7.12 (d, *J* = 2.18 Hz, 1H), 8.49 (s, 1H). ¹H NMR (DMSO-*d*₆) δ 6.63–6.65 (d, *J* = 8.4 Hz, 1H), 6.66–6.68 (d, *J* = 7.9 Hz, 1H), 6.74–6.76 (dd, *J*₁ = 8.4 Hz, *J*₂ = 1.85 Hz, 1H), 6.85–6.87 (dd, *J*₁ = 7.9 Hz, *J*₂ = 1.85 Hz, 1H), 7.00 (d, *J* = 1.85 Hz, 1H), 7.06 (d, *J* = 1.9 Hz, 1H), 7.93 (br s, 2H), 8.47 (s, 1H).

4,4'-(6-Aminopyrido[2,3-*b*]pyrazine-2,3-diyl)dibenzene-1,2-diol Dihydrochloride Salt (30). 2,3,6-Triaminopyridine dichloride (1.97 g, 10.0 mmol) and 3,3',4,4'-tetrahydroxybenzil (2.74 g, 10.0 mmol) were dissolved in 60 mL of 1:1 mixture of dioxane/water. The reaction mixture was refluxed for 18 h. Then solvent was removed *in vacuo* to give a dark-brown residue. The residue was dissolved in 20 mL of methanol and added dropwise with vigorous stirring to 500 mL of diethyl ether. The resulting brown precipitate was collected, redissolved in 20 mL of MeOH, and added again dropwise to 500 mL of anhydrous diethyl ether. The formed dark-yellow precipitate was centrifuged down, washed repeatedly with diethyl ether, and dried *in vacuo* to give the title compound **30** (3.96 g, 85.6%) as yellow solid, 98.2% purity by LC/MS (230 DAD). MS *m/z* [MH⁺] = 363.5. ¹H NMR (MeOH-*d*₄) δ 6.70–6.71 (d, *J* = 8.2 Hz, 1H), 6.73–6.75 (d, *J* = 8.1 Hz, 1H), 6.81–6.83 (dd, *J*₁ = 8.2 Hz, *J*₂ = 2.0 Hz, 1H), 6.90–6.92 (dd, *J*₁ = 8.1 Hz, *J*₂ = 2.0 Hz, 1H), 6.96 (d, *J* = 2.0 Hz, 1H), 7.07 (d, *J* = 2.0 Hz, 1H), 7.27–7.29 (d, *J* = 9.5 Hz, 1H), 8.34–8.36 (d, *J* = 9.5 Hz, 1H). ¹H NMR (DMSO-*d*₆) δ 6.67–6.71 (m, 3H), 6.75–6.77 (dd, *J*₁ = 8.3 Hz, *J*₂ = 2.1 Hz, 1H), 6.95 (d, *J* = 1.4 Hz, 1H), 7.05

(d, *J* = 2.1 Hz, 1H), 7.34–7.35 (d, *J* = 9.5 Hz, 1H), 8.37–8.39 (d, *J* = 9.5 Hz, 1H), 8.56 (br s, 1H), 9.65 (br s, 1H). Anal. (C₁₉H₁₄N₄O₄·2HCl·1.5H₂O) C, H, N.

4,4'-(8-Aminopyrido[3,4-*b*]pyrazine-2,3-diyl)diphenol Hydrochloride Salt (31). 3,4,5-Triaminopyridine trihydrochloride (2.6 g, 11.1 mmol) and 4,4'-dihydroxybenzil (2.83 g, 11.7 mmol) were dissolved in 60 mL of 1:1 mixture of dioxane/water. The reaction mixture was refluxed for 18 h. Then solvent was removed *in vacuo*. The resulting dark-brown residue was dissolved in ca. 50 mL of MeOH, and this solution was added dropwise to 1 L of diethyl ether with vigorous stirring. The formed solid was centrifuged down, washed repeatedly with diethyl ether, and dried *in vacuo* to give the title compound **31** (4.11 g, 91.9% yield) as dark-yellow solid, 97.7% purity by LC/MS (ELSD). MS *m/z* [MH⁺] = 331.5. ¹H NMR (DMSO-*d*₆) δ 6.78–6.83 (m, 4H), 7.40–7.43 (m, 2H), 7.57–7.60 (m, 2H), 7.98 (d, *J* = 0.76 Hz, 1H), 8.85 (d, *J* = 0.76 Hz, 1H), 10.2 (br s, 2H). Anal. (C₁₉H₁₄N₄O₂·1HCl·2H₂O) C, H, N.

4,4'-(6-Aminopyrido[2,3-*b*]pyrazine-2,3-diyl)diphenol (32). 2,3,6-Triaminopyridine dihydrochloride (1.97 g, 10.0 mmol) and 4,4'-dihydroxybenzil (2.42 g, 10.0 mmol) were dissolved in 60 mL of 1:1 mixture of dioxane/water. The reaction mixture was refluxed for 18 h. Then solvent was removed *in vacuo*. The resulting dark-brown residue was dissolved in ca. 20 mL of MeOH, and this solution was added dropwise to 1 L of diethyl ether with vigorous stirring. The formed solid was centrifuged down, washed repeatedly with diethyl ether, and dried *in vacuo* to give the title compound **32** (3.29 g, 85.4% yield) as dark-yellow solid, 94.7% purity by LC/MS (230 nm). MS *m/z* [MH⁺] = 331.5, 332.5. ¹H NMR (MeOH-*d*₄) δ 6.74–6.78 (m, 4H), 7.29–7.31 (d, *J* = 9.5 Hz, 1H), 7.34–7.36 (m, 2H), 7.43–7.45 (m, 2H), 8.39–8.40 (d, *J* = 9.5 Hz, 1H). ¹H NMR (DMSO-*d*₆) δ 6.75–6.77 (d, *J* = 5.9 Hz, 2H), 6.77–6.78 (d, *J* = 5.9 Hz, 2H), 7.23–7.24 (d, *J* = 8.7 Hz, 2H), 7.29–7.31 (d, *J* = 8.7 Hz, 2H), 7.38–7.40 (d, *J* = 9.5 Hz, 1H), 8.38–8.40 (d, *J* = 9.5 Hz, 1H), 8.68 (br s, 1H), 9.71 (br s, 1H), 9.87 (br s, 1H), 10.07 (br s, 1H). Anal. (C₁₉H₁₄N₄O₂·1.5HCl) C, H, N.

4-(4-Aminopteridin-7-yl)benzene-1,2-diol (33). This compound is made by stirring a 1:1 ratio of 3,4-dihydroxyphenylglyoxal with the free base of 2,4,5,6-tetraaminopyrimidine in water at a pH of 7 for ca. 3 h. The product was isolated by filtering the precipitated free base, washing sequentially with water (2 × 40 mL), methanol (1 × 40 mL), and ether (2 × 40 mL), and drying in a vacuum desiccator. ¹H NMR (500 MHz; DMSO-*d*₆): δ 6.92 (d, *J* = 8.3 Hz, 1 H), 7.71 Hz, (dd, *J* = 8.4 Hz, *J* = 2.3 Hz, 1 H), 7.80 (d, *J* = 2.3 Hz, 1 H), 8.17 (br s, 1 H), 8.12 (br s, 1 H), 8.51 (s, 1 H), 9.28 (s, 1 H), 9.40 (br s, 1 H), 9.72 (s, 1 H).

4-(4-Aminopteridin-6-yl)benzene-1,2-diol (34). The same synthetic procedure as for compound **19**, 98.7% purity (92:8 ratio of regioisomers) by LC/MS (230 DAD), ELSD purity 100%. MS *m/z* [MH⁺] = 256.1. ¹H NMR (DMSO-*d*₆) for major regioisomer δ 6.89 (dd, *J*₁ = 7.9 Hz, *J*₂ = 2.1 Hz, 1H), 7.82 (d, *J* = 2.1 Hz, 1H), 8.11 (br s, 1H), 8.22 (br s, 1H), 8.49 (br s, 1H), 9.08 (br s, 1H), 9.52 (s, 1H), 9.70 (br s, 1H).

Acknowledgment. We thank Chris Jacob, Antonio Boccia, and Jann Key for assistance in the animal experiments and Kathy Barrett and Tessa Chung for assistance in the execution of various cell culture and biochemical assays.

Supporting Information Available: Elemental analyses data. This material is available free of charge via the Internet at <http://pubs.acs.org>.

References

- (1) (a) Senger, D. R.; Galli, S. J.; Dvorak, A. M.; Perruzzi, C. A.; Harvey, V. S.; Dvorak, H. F. Tumor cells secrete a vascular permeability factor that promotes accumulation of ascites fluid. *Science* **1983**, *219*, 983–985.
- (2) Pratt, D. J.; Endicott, J. A.; Noble, M. E. The role of structure in kinase-targeted inhibitor design. *Curr. Opin. Drug Discovery Dev.* **2004**, *7*, 428–436.

- (3) Mecklenbrauker, I.; Kalled, S. L.; Leitges, M.; Mackay, F.; Tarakhovskiy, A. Regulation of B-cell survival by BAFF-dependent PKC δ mediated nuclear signaling. *Nature* **2004**, *431*, 456–461.
- (4) Kinzel, V.; Mueller, G. C. Phosphorylation of surface proteins of HeLa cells using an exogenous protein kinase and (gamma-32P)-ATP. *Biochim. Biophys. Acta* **1973**, *322*, 337–351.
- (5) Dancey, J.; Sausville, E. A. Issues and progress with protein kinase inhibitors for cancer treatment. *Nat. Rev. Drug Discovery* **2003**, *2*, 296–313.
- (6) Ishizawa, R.; Parsons, S. J. c-Src and cooperating partners in human cancer. *Cancer Cell* **2004**, *6*, 209–214.
- (7) Olmsted, J. B.; Borisy, G. G. Microtubules. *Annu. Rev. Biochem.* **1973**, *42*, 507–540.
- (8) Bitensky, M. W.; Gorman, R. E. Cellular responses to cyclic AMP. *Prog. Biophys. Mol. Biol.* **1973**, *26*, 409–461.
- (9) Shin, N. Y.; Dize, R. S.; Schneider-Mergener, J.; Ritchie, M. D.; Kilkenny, D. M.; Hanks, S. K. Subsets of the major phosphorylation sites in Crk-associated substrate (CAS) are sufficient to promote cell migration. *J. Biol. Chem.* **2004**, *279*, 38331–38337.
- (10) Frey, M. R.; Golovin, A.; Polk, D. B. Epidermal growth factor-stimulated intestinal epithelial cell migration requires Src family kinase-dependent p38 MAPK signaling. *J. Biol. Chem.* **2004**, *279*, 44513–44521.
- (11) McConkey, D. J.; Hartzell, P.; Jondal, M.; Orrenius, S. Inhibition of DNA fragmentation in thymocytes and isolated thymocyte nuclei by agents that stimulate protein kinase C. *J. Biol. Chem.* **1989**, *264*, 13399–13402.
- (12) Lee, M.; Kim, J. Y.; Koh, W. S. Apoptotic effect of PP2 a Src tyrosine kinase inhibitor, in murine B cell leukemia. *J. Cell Biochem.* **2004**, *93*, 629–638.
- (13) Gruber, C.; Henkel, M.; Budach, W.; Belka, C.; Jendrossek, V. Involvement of tyrosine kinase p56/Lck in apoptosis induction by anticancer drugs. *Biochem. Pharmacol.* **2004**, *67*, 1859–1872.
- (14) Park, S. S.; Eom, Y. W.; Kim, E. H.; Lee, J. H.; Min do, S.; Kim, S.; Choi, K. S. Involvement of c-Src kinase in the regulation of TGF-beta1-induced apoptosis. *Oncogene* **2004**, *23*, 6272–6281.
- (15) Shelton, J. G.; Moyer, P. W.; Steelman, L. S.; Blalock, W. L.; Lee, J. T.; Franklin, R. A.; McMahon, M.; McCubrey, J. A. Differential effects of kinase cascade inhibitors on neoplastic and cytokine-mediated cell proliferation. *Leukemia* **2003**, *17*, 1765–1782.
- (16) Gschwind, A.; Fischer, O. M.; Ullrich, A. The discovery of receptor tyrosine kinases: targets for cancer therapy. *Nat. Rev. Cancer* **2004**, *4*, 361–370.
- (17) Cines, D. B.; Pollak, E. S.; Buck, C. A.; Loscalzo, J.; Zimmerman, G. A.; McEver, R. P.; Pober, J. S.; Wick, T. M.; Konkle, B. A.; Schwartz, B. S.; Barnathan, E. S.; McCrae, K. R.; Hug, B. A.; Schmidt, A. M.; Stern, D. M. Endothelial cells in physiology and in the pathophysiology of vascular disorders. *Blood* **1998**, *91*, 3527–3561.
- (18) Weis, S.; Shintani, S.; Weber, A.; Kirchmair, R.; Wood, M.; Cravens, A.; McSharry, H.; Iwakura, A.; Yoon, Y. S.; Himes, N.; Burstein, D.; Doukas, J.; Soll, R.; Losordo, D.; Cheresch, D. Src blockade stabilizes a Flk/cadherin complex, reducing edema and tissue injury following myocardial infarction. *J. Clin. Invest.* **2004**, *113*, 885–894.
- (19) Paul, R.; Zhang, Z. G.; Eliceiri, B. P.; Jiang, Q.; Boccia, A. D.; Zhang, R. L.; Chopp, M.; Cheresch, D. Src deficiency or blockade of Src activity in mice provides cerebral protection following stroke. *Nat. Med.* **2001**, *7*, 222–227.
- (20) Hanke, J. H.; Gardner, J. P.; Dow, R. L.; Changelian, P. S.; Brissette, W. H.; Weringer, E. J.; Pollok, B. A.; Connelly, P. A. Discovery of a novel, potent, and Src family-selective tyrosine kinase inhibitor. Study of Lck- and FynT-dependent T cell activation. *J. Biol. Chem.* **1996**, *271*, 695–701.
- (21) Warmuth, M.; Damoiseaux, R.; Liu, Y.; Fabbro, D.; Gray, N. Src family kinases: potential targets for the treatment of human cancer and leukemia. *Curr. Pharm. Des.* **2003**, *9*, 2043–2059.
- (22) Tsygankov, A. Y.; Shore, S. K. Src: regulation, role in human carcinogenesis and pharmacological inhibitors. *Curr. Pharm. Des.* **2004**, *10*, 1745–1756.
- (23) Levin, V. A. Basis and importance of Src as a target in cancer. *Cancer Treat. Res.* **2004**, *119*, 89–119.
- (24) Creemer, L. C.; Kirst, H. A.; Vlahos, C. J.; Schultz, R. M. Synthesis and *In Vitro* Evaluation of New Wortmannin Esters: Potent Inhibitors of Phosphatidylinositol 3-Kinase. *J. Med. Chem.* **1996**, *39*, 5021–5024.
- (25) Vivanco, I.; Sawyers, C. L. The phosphatidylinositol 3-Kinase Akt pathway in human cancer. *Nat. Rev. Cancer* **2002**, *2*, 489–501.
- (26) Stein, R. C.; Waterfield, M. D. PI3-kinase inhibition: a target for drug development? *Mol. Med. Today* **2000**, *6*, 347–357.
- (27) Walker, E. H.; Pacold, M. E.; Perisic, O.; Stephens, L.; Hawkins, P. T.; Wymann, M. P.; Williams, R. L. Structural determinants of phosphoinositide 3-kinase inhibition by Wortmannin. LY294002, quercetin, myricetin, and staurosporine. *Mol. Cell* **2000**, *6*, 909–919.
- (28) Zhu, T.; Gu, J.; Yu, K.; Lucas, J.; Cai, P.; Tsao, R.; Gong, Y.; Li, F.; Chaudhary, I.; Desai, P.; Ruppen, M.; Fawzi, M.; Gibbons, J.; Ayrall-Kaloustian, S.; Skotnicki, J.; Mansour, T.; Zask, A.; Pegylated Wortmannin and 17-Hydroxywortmannin Conjugates as Phosphoinositide 3-Kinase Inhibitors Active in Human Tumor Xenograft Models. *J. Med. Chem.* **2006**, *49*, 1373–1378.
- (29) Gammill, R. B.; Judge, T. M.; Morris, J. Preparation of antiatherosclerotic and antithrombotic 1-benzopyran-4-ones and 2-amino-1,3-benzoxazine-4-ones. PCT Int. Appl. WO9119707, 1991.
- (30) Gogliotti, R. D.; Muccioli, K. L.; Para, K. S.; Visnick, M. Preparation of benzoxazines and related compounds as inhibitors of PI3Ks. PCT Int. Appl. WO2004056820, 2004.
- (31) Connolly, M. K.; Gogliotti, R. D.; Hurt, C. R.; Reichard, G. A.; Visnick, M. Preparation of halo-substituted N-tetrazolylbenzo[b]-thiophenecarboxamides with PI3K inhibitory activity as therapeutic agents. PCT Int. Appl. WO2005023800, 2005.
- (32) Gogliotti, R. D.; Lee, H. T.; Sexton, K. E.; Visnick, M. Preparation of tetrazolyl benzofurancarboxamides as phosphoinositide-3-kinase (PI3K) inhibitors for the treatment of cancer, inflammatory and cardiovascular diseases. PCT Int. Appl. WO2004108709, 2004.
- (33) Connolly, M. K.; Gogliotti, R. D.; Plummer, M. S.; Visnick, M. Preparation of morpholinyl-pyrimidine derivatives as inhibitors of phosphoinositide-3-kinases. PCT Int. Appl. WO2005042519, 2005.
- (34) Shimada, M.; Murata, T.; Fuchikami, K.; Tsujishita, H.; Omori, N.; Kato, I.; Miura, M.; Urbahns, K.; Gantner, F.; Bacon, K. Preparation of fused azole-pyrimidine derivatives as PI3K inhibitors with therapeutic uses. PCT Int. Appl. WO2004029055, 2004.
- (35) Bagli, E.; Stefanidou, M.; Morbidelli, L.; Ziche, M.; Psillas, K.; Murphy, C.; Fotsis, T. Luteolin inhibits vascular endothelial growth factor-induced angiogenesis; inhibition of endothelial cell survival and proliferation by targeting phosphatidylinositol 3'-kinase activity. *Cancer Res.* **2004**, *64*, 7936–7946.
- (36) Wang, S.; Dusting, G. J.; May, C. N.; Woodman, O. L. 3',4'-Dihydroxyflavonol reduces infarct size and injury associated with myocardial ischaemia and reperfusion in sheep. *Br. J. Pharmacol.* **2004**, *142*, 443–452.
- (37) Suzuki, M.; Tabuchi, M.; Ikeda, M.; Umegaki, K.; Tomita, T. Protective effects of green tea catechins on cerebral ischemic damage. *Med. Sci. Monit.* **2004**, *10*, 166–174.
- (38) Kiziltepe, U.; Turan, N. N.; Han, U.; Ulus, A. T.; Akar, F. Resveratrol, a red wine polyphenol, protects spinal cord from ischemia-reperfusion injury. *J. Vasc. Surg.* **2004**, *40*, 138–145.
- (39) Choi, Y. B.; Kim, Y. I.; Lee, L. S.; Kim, B. S.; Kim, D. J. Protective effect of epigallocatechin gallate on brain damage after transient middle cerebral artery occlusion in rats. *Brain Res.* **2004**, *1019*, 47–54.
- (40) Li, X. L.; Li, Y. Q.; Yan, W. M.; Li, H. Y.; Xu, H.; Zheng, X. X.; Guo, D. W.; Tang, L. K. A study of the cardioprotective effect of breviscapine during hypoxia of cardiomyocytes. *Planta Med.* **2004**, *70*, 1039–1044.
- (41) Graboyes, H.; Day, A. R. Metabolite Analogs. VIII. Syntheses of some imidazolopyridines and pyridotriazoles. *J. Am. Chem. Soc.* **1957**, *79*, 6421–6426.
- (42) Ohmori, J.; Kubota, H.; Shimizu-Sasamata, M.; Okada, M.; Sakamoto, S. Novel α -amino-3-hydroxy-5-methylisoxazole-4-propionate receptor antagonists: synthesis and structure-activity relationships of 6-(1H-imidazol-1-yl)-7-nitro-2,3(1H,4H)-pyrido[2,3-b]pyrazinedione and related compounds. *J. Med. Chem.* **1996**, *39*, 1331–1338.
- (43) (a) Taylor, E. C.; Perlman, K. L.; Kim, Y. H.; Sword, I. P.; Jacobi, P. A. Pteridines. XXIX. An unequivocal route to 2,4-diamino-6-substituted pteridines. *J. Am. Chem. Soc.* **1973**, *95*, 6413–6418. (b) Taylor, E. C.; Ray, P. S. Pteridines. 51. A new and unequivocal route to C-6 carbon-substituted pterins and pteridines. *J. Org. Chem.* **1987**, *52*, 3997–4000.
- (44) (a) De Meester, J. W. G.; van der Plas, H. C. The oxidation of 6- and 7-Aryl-4(3H)-pteridinones by immobilized arthrobacter M-4 cells containing xanthine oxidase. *J. Heterocycl. Chem.* **1987**, *24*, 441–452. (b) Campillo, N.; Goya, P.; Paez, J. A. Novel arylpyrazino-[2,3-c][1,2,6]thiadiazine 2,2-dioxides as platelet aggregation inhibitors. 2. Optimization by quantitative structure–activity relationships. *J. Med. Chem.* **1999**, *42*, 3279–3288. (c) Ishikawa, T. Product class 21: pteridines and related structures. *Sci. Synth.* **2004**, *16*, 1291–1335.

- (45) (a) Yamamoto, H.; Hutzenlaub, W.; Pfeleiderer, W. Synthesis and properties of pterin- and 2,6-diamino-pteridine-mono and di-N-oxides. *Chem. Ber.* **1973**, *106*, 3175–3193. (b) Taghavi-Moghadam, S.; Pfeleiderer, W. A new general and regioselective method for the synthesis of 2,4-disubstituted 4-amino-pteridines. *Tetrahedron Lett.* **1997**, *39*, 6835–6836.
- (46) Kim, Y.; Kang, Y.; Baek, D. Oxidative synthesis of benzoylpteridines from benzylpteridines by potassium permanganate. *Bull. Korean Chem. Soc.* **2001**, *22*, 141–144.
- (47) Gavard, J.; Gutkind, J. S. VEGF controls endothelial-cell permeability by promoting the beta-arrestin-dependent endocytosis of VE-cadherin. *Nat. Cell. Biol.* **2006**, *8*, 1223–1234.
- (48) Brkovic, A.; Sirois, M. G. Vascular permeability induced by VEGF family members in vivo: role of endogenous PAF and NO synthesis. *J. Cell Biochem.* **2007**, *100*, 727–737.
- (49) Bateman, R. M.; Tokunaga C.; Kareco, T.; Dorscheid, D. R.; Walley, K. R. Myocardial hypoxia-inducible HIF-1 α , VEGF and GLUT1 gene expression is associated with microvascular and ICAM-1 heterogeneity during endotoxemia. *Am J. Physiol Heart Circ. Physiol.* **2007**, *293*, H448–456.
- (50) Hasebe, Y.; Egawa, K.; Yamazaki, Y.; Kunimoto, S.; Hirai, Y.; Ida, Y.; Nose, K. Specific inhibition of hypoxia-inducible factor (HIF)-1 alpha activation and of vascular endothelial growth factor (VEGF) production by flavonoids. *Biol. Pharm. Bull.* **2003**, *26*, 1379–1383.
- (51) Duarte, J.; Jimenez, R.; O'Valle, F.; Galisteo, M.; Perez-Palencia, R.; Vargas, F.; Perez-Vizcaino, F.; Zarzuelo, A.; Tamargo, J. Protective effects of the flavonoid quercetin in chronic nitric oxide deficient rats. *J. Hypertens.* **2002**, *20*, 1843–1854.
- (52) Yuan, S. Y. Protein kinase signaling in the modulation of microvascular permeability. *Vascul. Pharmacol.* **2002**, *39*, 213–223.
- (53) The antibodies used in this study for Western blotting were from Santa Cruz Biotechnology; catalog no. sc-6548, Santa Cruz, CA (antibody to VE-Cadherin), and Chemicon; catalog no. APT-184, Temecula, CA (Omni-Phos, and pan-phosphorylated proteins).
- (54) Doukas, J.; Wrasidlo, W.; Noronha, G.; Dneprovskaia, E.; Fine, R.; Weis, S.; Hood, J.; Demaria, A.; Soll, R.; Cheresch, D. Phosphoinositide 3-kinase gamma/delta inhibition limits infarct size after myocardial ischemia/reperfusion injury. *Proc. Natl. Acad. Sci. U.S.A.* **2006**, *103*, 19866–71. Briefly, cell proliferation assays was carried out using human umbilical vein EC plated in 96-well cluster plates (5000 cells/well) were cultured in assay medium (containing 0.5% serum and 50 ng/ml VEGF) in the presence or absence of test compounds (10 μ M), and cell numbers were quantified by XTT assay (Promega, Madison, WI) after 24, 48, or 72 h later.
- (55) Kinexus provides antibody microarray services that would examine cell lysates using 377 pan-specific and 273 phospho-site-specific antibodies. The proteomics service provides information on protein expression, phosphorylation, and protein-protein expression from cell lysates. This technique would allow one to examine the kinases that were affected by a compound. The complete details are provided at their web site (www.kinexus.ca). Kinexus technology would allow one to examine numerous pathways. Visit their web site for more information. The concentration of compound **6** was 10 μ M in cell assays.
- (56) Hu, E.; Mueller, E.; Oliviero, S.; Papaioannou, V. E.; Johnson, R.; Spiegelman, B. M. Targeted disruption of the c-Fos gene demonstrates c-Fos-dependent and -independent pathways for gene expression stimulated by growth factors or oncogenes. *EMBO J.* **1994**, *13*, 3094–3103.
- (57) Frohlich, L. G.; Kotsonis, P.; Traub, H.; Taghavi-Moghadam, S.; Al-Masoudi, N.; Hofmann, H.; Strobel, H.; Matter, H.; Pfeleiderer, W.; Schmidt, H. H. H. W. Inhibition of neuronal nitric oxide synthase by 4-amino pteridine derivatives: structure-activity relationship of antagonists of (6R)-5,6,7,8-tetrahydrobiopterin Cofactor. *J. Med. Chem.* **1999**, *42*, 4108–4121.
- (58) Doukas, J.; Wrasidlo, W.; Noronha, G.; Dneprovskaia, E.; Fine, R.; Weis, S.; Hood, J.; Demaria, A.; Soll, R.; Cheresch, D. Phosphoinositide 3-kinase gamma/delta inhibition limits infarct size after myocardial ischemia/reperfusion injury. *Proc. Natl. Acad. Sci. U.S.A.* **2006**, *103*, 19866–71.
- (59) Laffargue, M.; Calvez, R.; Finan, P.; Trifilieff, A.; Barbier, M.; Altruda, F.; Hirsch, E.; Wymann, M. P. Phosphoinositide 3-kinase γ is an essential amplifier of mast cell function. *Immunity* **2002**, *16*, 441–451.
- (60) We have tested compound **6** against 140 kinases at a single concentration of 10 μ M in DMSO at UpState (www.upstate.com). Kinases inhibited at greater than 90% were selected for IC₅₀ determinations. Compound **6** potently inhibited the β , δ , and γ isoforms of PI3K. Apart from the PI3K isoforms, compound **6** also inhibited AAK1, BIKE, CLK1, CLK2, CLK3, PKC μ , RIPK2, and Tie2. This information is provided as supplementary material (Appendix A).
- (61) DISCOVER, Insight II and the CFF force field are trademarked software offerings from Accelrys Inc., San Diego, CA.
- (62) Manuscript in preparation.
- (63) <http://clinicaltrials.gov/ct/show/NCT00103350?order=1>.
- (64) YASARA is a trademarked software offering of Yasara Biosciences, Austria.
- (65) (a) Ferby, I. M.; Waga, I.; Hoshino, M.; Kume, K.; Shimizu, T. Wortmannin inhibits mitogen-activated protein kinase activation by platelet-activating factor through a mechanism independent of p85/p110-type phosphatidylinositol 3-kinase. *J. Biol. Chem.* **1996**, *271*, 11684–11688. (b) Nakanishi, S.; Kakita, S.; Takahashi, I.; Kawahara, K.; Tsukuda, E.; Sano, T.; Yamada, K.; Yoshida, M.; Kase, H.; Matsuda, Y. Wortmannin, a microbial product inhibitor of myosin light chain kinase. *J. Biol. Chem.* **1992**, *267*, 2157–2163. (c) Vanhaesebroeck, B.; Leever, S. J.; Ahmadi, K.; Timms, J.; Katso, R.; Driscoll, P. C.; Woscholski, R.; Parker, P. J.; Waterfield, M. D. Synthesis and function of 3-phosphorylated inositol lipids. *Annu. Rev. Biochem.* **2001**, *70*, 535–602.
- (66) Camps, M.; Ruckle, T.; Ji, H.; Ardisson, V.; Rintelen, F.; Shaw, J.; Ferrandi, C.; Chabert, C.; Gillieron, C.; Francon, B.; Martin, T.; Gretener, D.; Perrin, D.; Leroy, D.; Vitte, P. A.; Hirsch, E.; Wymann, M. P.; Cirillo, R.; Schwarz, M. K.; Rommel, C. Blockade of PI3K γ suppresses joint inflammation and damage in mouse models of rheumatoid arthritis. *Nat. Med.* **2005**, *11*, 936–943.
- (67) Poh, T. W.; Pervaiz, S. LY294002 and LY303511 sensitize tumor cells to drug-induced apoptosis via intracellular hydrogen peroxide production independent of the phosphoinositide 3-kinase-Akt pathway. *Cancer Res.* **2005**, *65*, 6264–6274.
- (68) Lesk, A. M. Extraction of well-fitting substructures: root-mean-square deviation and the difference distance matrix. *Fold. Des.* **1997**, *2* (3), S12–4.
- (69) Duncan, B. S.; Olson, A. J. Shape analysis of molecular surfaces. *Biopolymers* **1993**, *2*, 231–238.

JM051056C